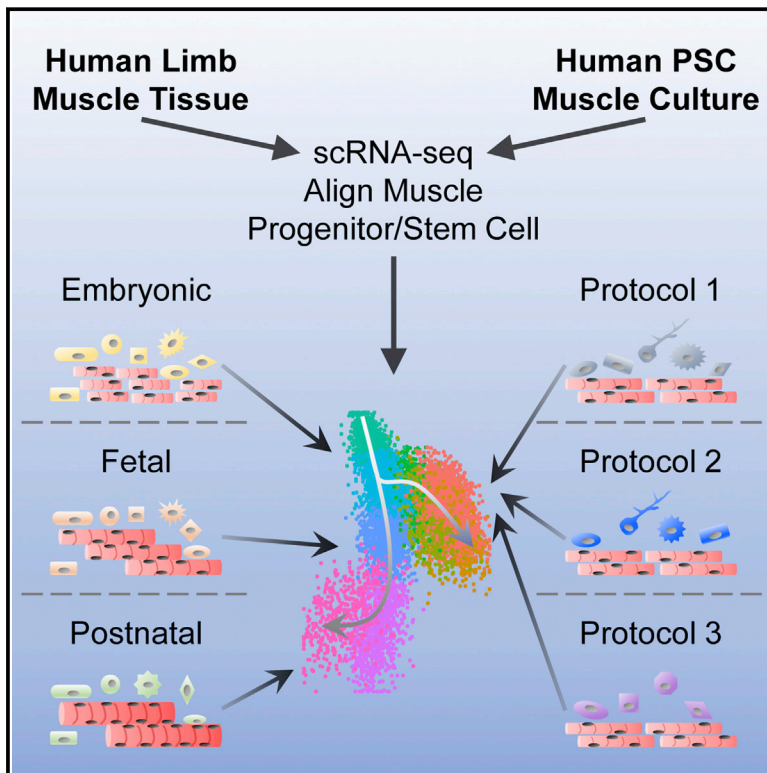# Cell Stem Cell

A Human Skeletal Muscle Atlas Identifies the Trajectories of Stem and Progenitor Cells across Development and from Human Pluripotent Stem Cells

Graphical Abstract

Authors
Haibin Xi, Justin Langerman, Shan Sabri, ..., Katja Schenke-Layland, Kathrin Plath, April D. Pyle

Correspondence
kplath@mednet.ucla.edu (K.P.),
apyle@mednet.ucla.edu (A.D.P.)

In Brief
Xi et al. developed a comprehensive view of skeletal muscle and supportive cells across human development. This atlas revealed transcriptional differences among myogenic progenitors and stem cells at distinct developmental stages. This enabled identification of the developmental status of hPSC-derived muscle cells to the embryonic-to-fetal transition period in human development.

Highlights
- Human atlas of limb skeletal muscle in embryonic, fetal, and adult tissues
- Human limb skeletal muscle populations and supportive cells vary across development
- PAX7 muscle progenitor and stem cells are not identical across developmental states
- hPSC-PAX7 cells align to the embryonic-to-fetal transition in human development

CellPress

Resource

A Human Skeletal Muscle Atlas Identifies the Trajectories of Stem and Progenitor Cells across Development and from Human Pluripotent Stem Cells

Haibin Xi,[1,2] Justin Langerman,[3] Shan Sabri,[3] Peggie Chien,[1,2,4] Courtney S. Young,[5,13] Shahab Younesi,[1,2] Michael Hicks,[1,2] Karen Gonzalez,[6,14] Wakana Fujiwara,[7,15] Julia Marzi,[8,9] Simone Liebscher,[8] Melissa Spencer,[2,4,5] Ben Van Handel,[10] Denis Evseenko,[10] Katja Schenke-Layland,[8,9,11] Kathrin Plath,[2,3,4,12,*] and April D. Pyle[1,2,4,12,16,*]

[1]Department of Microbiology, Immunology, and Molecular Genetics, University of California, Los Angeles, Los Angeles, CA, USA
[2]Eli and Edythe Broad Center of Regenerative Medicine and Stem Cell Research, University of California, Los Angeles, Los Angeles, CA, USA
[3]Deparment of Biological Chemistry, David Geffen School of Medicine, University of California, Los Angeles, Los Angeles, CA, USA
[4]Molecular Biology Institute, University of California, Los Angeles, Los Angeles, CA, USA
[5]Department of Neurology, University of California, Los Angeles, Los Angeles, CA, USA
[6]Department of Molecular, Cell and Developmental Biology, University of California, Los Angeles, Los Angeles, CA, USA
[7]Department of Biochemistry, University of California, Los Angeles, Los Angeles, CA, USA
[8]Department of Women's Health, Research Institute for Women's Health, Eberhard Karls University Tübingen, Tübingen, Germany
[9]The Natural and Medical Sciences Institute (NMI) at the University of Tübingen, Reutlingen, Germany
[10]Department of Orthopaedic Surgery, Keck School of Medicine, Stem Cell Research and Regenerative Medicine, University of Southern California, Los Angeles, CA, USA
[11]Department of Medicine/Cardiology, Cardiovascular Research Laboratories, University of California, Los Angeles, Los Angeles, CA, USA
[12]Jonsson Comprehensive Cancer Center, University of California, Los Angeles, Los Angeles, CA, USA
[13]Present address: MyoGene Bio, Los Angeles, CA, USA
[14]Present address: Institute for Stem Cell Biology and Regenerative Medicine and Department of Biology, Stanford University, Stanford, CA, USA
[15]Present address: Georgetown University School of Medicine, Washington, D.C., USA
[16]Lead Contact
*Correspondence: kplath@mednet.ucla.edu (K.P.), apyle@mednet.ucla.edu (A.D.P.)
https://doi.org/10.1016/j.stem.2020.04.017

SUMMARY

The developmental trajectory of human skeletal myogenesis and the transition between progenitor and stem cell states are unclear. We used single-cell RNA sequencing to profile human skeletal muscle tissues from embryonic, fetal, and postnatal stages. *In silico*, we identified myogenic as well as other cell types and constructed a "roadmap" of human skeletal muscle ontogeny across development. In a similar fashion, we also profiled the heterogeneous cell cultures generated from multiple human pluripotent stem cell (hPSC) myogenic differentiation protocols and mapped hPSC-derived myogenic progenitors to an embryonic-to-fetal transition period. We found differentially enriched biological processes and discovered co-regulated gene networks and transcription factors present at distinct myogenic stages. This work serves as a resource for advancing our knowledge of human myogenesis. It also provides a tool for a better understanding of hPSC-derived myogenic progenitors for translational applications in skeletal muscle-based regenerative medicine.

INTRODUCTION

Skeletal myogenesis starts early during development, which initially gives rise to prenatal skeletal muscle progenitor cells (SMPCs) and later on postnatal satellite cells (SCs) (Applebaum and Kalcheim, 2015; Cerletti et al., 2008; Chal and Pourquié, 2017; Sambasivan and Tajbakhsh, 2007). Both populations are endowed with muscle stem cell properties, including, in addition to the expression of the essential myogenic transcription factor (TF) PAX7, the ability to expand and fuse to generate new myofibers *in vitro* or *in vivo* (Sacco et al., 2008; Tierney et al., 2016). However, the molecular and functional differences between SMPCs and SCs are only beginning to be unveiled. *In vivo*, mouse SMPCs contribute to muscle establishment and growth, whereas SCs in mature muscles are typically quiescent and enter the cell cycle in the event of injury (Tierney and Sacco, 2016). *In vitro*, isolated mouse SMPCs proliferate and maintain PAX7 expression longer than SCs. Moreover, following transplantation after muscle injury, mouse SCs are superior to fetal SMPCs to repopulate the stem cell niche and support long-term regeneration (Tierney et al., 2016). Despite studies of developmental myogenesis in model
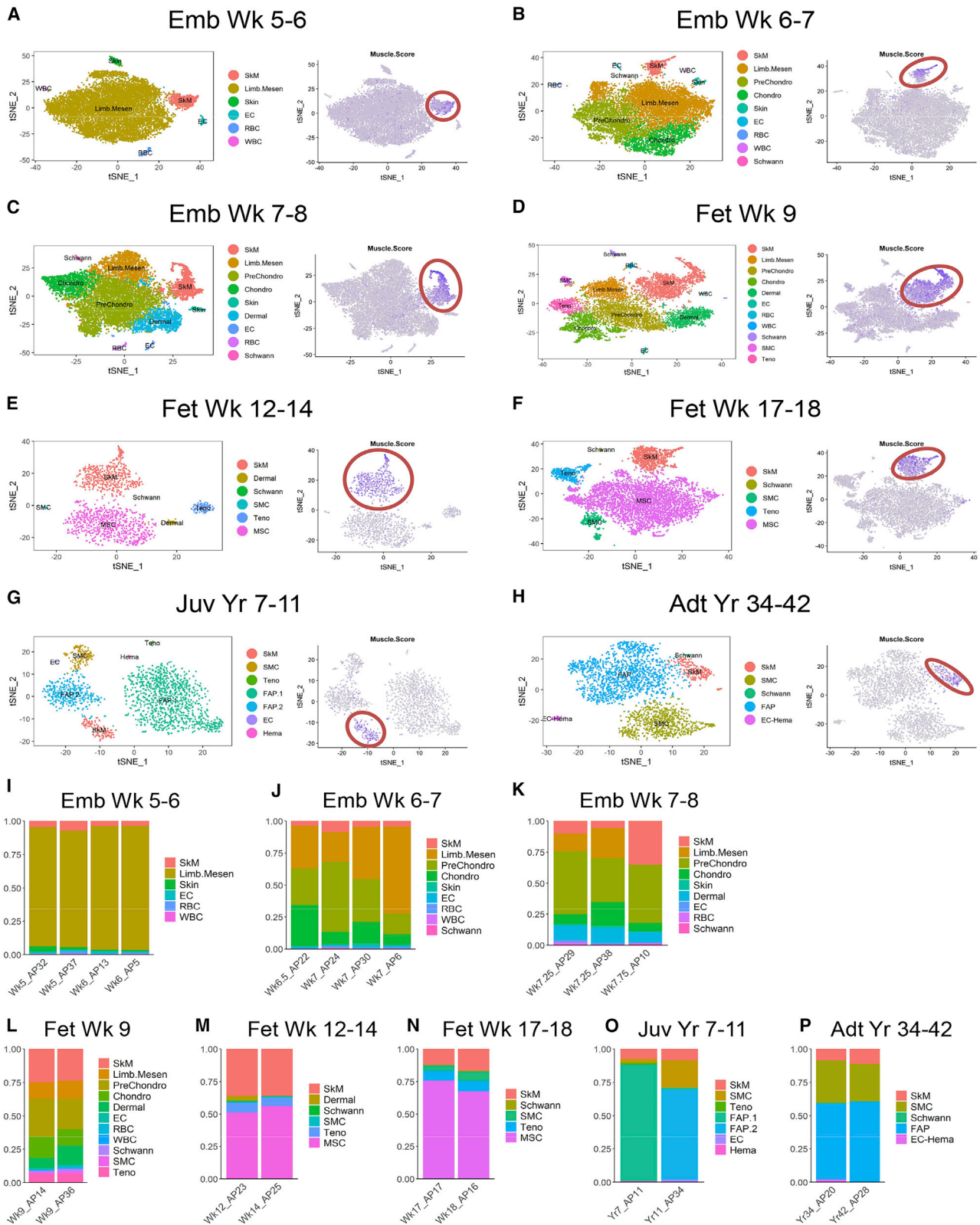
(legend on next page)

organisms, our knowledge of muscle ontogeny in human is limited (Schiaffino et al., 2015).

Following developmental cues, we and others have developed directed differentiation protocols using human pluripotent stem cells (hPSCs) to generate myogenic cells including SMPCs or SC-like cells (Borchin et al., 2013; Chal et al., 2015; Hicks et al., 2018; Magli and Perlingeiro, 2017; Shelton et al., 2014; Xi et al., 2017; Xu et al., 2013). These cells may serve as potential sources for personalized cell replacement therapies for degenerative muscle diseases or sarcopenia. However, they have not been fully characterized and compared with *in vivo* human SMPCs or SCs to facilitate their proper translation to clinical usage.

Here, we performed a comprehensive single-cell RNA sequencing (scRNA-seq) analysis of myogenesis in human limb tissues across development. We identified skeletal muscle (SkM) cells as well as other supportive cell types present at distinct developmental stages. We also evaluated the myogenic and non-myogenic cell populations from three different directed differentiation strategies from hPSCs. Using the developmental trajectory built from the *in vivo* SMPCs and SCs, we mapped hPSC-derived progenitor cells to a developmental period corresponding to the embryonic-to-fetal transition (7–12 weeks prenatal) across all protocols. Further analysis identified gene groups differentially regulated across developmental stages and provided potential TF candidates that may regulate stage transitions. In summary, this work provides a critical resource to understand the developmental networks defining human skeletal myogenesis and can be used to aid molecular identification of myogenic cells derived from hPSCs. This work will enable the development of new approaches to mature and support the most regenerative cells from hPSCs for use in cell-based therapies.

RESULTS

Identification of Skeletal Myogenic and Supportive Cell Types using ScRNA-Seq across *In Vivo* Human Development

To gain a comprehensive view of cell populations present during human SkM ontogeny, we used scRNA-seq to evaluate human limb muscle tissues from embryonic (weeks 5–8), fetal (weeks 9–18), and postnatal juvenile (years 7–11) and adult (years 34–42) stages (see STAR Methods; Table S1). To universally identify skeletal myogenic cells from different samples, we developed a computational tool called Muscle.Score that examines the average expression of a list of conserved genes representing myogenic cells of distinct developmental and differentiation status (*PAX3*, *PAX7*, *PITX2*, *MYF5*, *MYF6*, *MYOD1*, *MYOG*, *NEB*, and *MYH3*). Using Muscle.Score, we were able to readily identify SkM cells at each developmental stage (Figure 1). Within mono-

nucleated cells from whole limbs, SkM cells gradually increased in proportion from early embryonic stage (weeks 5–6; ~5%) to the beginning of fetal stage (week 9; above 20%) (Figures 1A–1D, 1I–1L, and S1I). At early fetal stage (weeks 12–14; ~35%), SkM cells constituted a major cell type of the non-endothelial/hematopoietic lineages in limbs (Figures 1E, 1M, and S1I). This proportion decreased during later fetal development (weeks 17–18; ~15%) and further dropped in postnatal juvenile and adult limb SkM tissues (below 10%) (Figures 1F–1H, 1N–1P, and S1I).

In addition to SkM cells, we also found various non-myogenic populations at distinct developmental time points. One highly dynamic population is formed by mesenchymal cell types. Early on (weeks 5–6), the mesenchyme of the developing limbs was relatively homogeneous, composed mainly of *DUSP6*+ multipotent limb mesenchymal progenitors (Limb.Mesen) (Gros and Tabin, 2014; Reinhardt et al., 2019) (Figures 1A, 1I, and S1A). As limbs developed (weeks 6–9), the multipotent progenitors became more lineage restricted, and *SHOX2*+ prechondrogenic (PreChondro) and *SOX9*+ chondrogenic (Chondro) progenitors became prominent (Akiyama et al., 2005; Barna and Niswander, 2007; Neufeld et al., 2014) (Figures 1B–1D, 1J–1L, and S1B–S1D). During fetal development (weeks 12–18), the mesenchymal cells expressed the mesenchymal stromal cell (MSC) marker *NT5E/CD73* (Figures 1E, 1F, 1M, 1N, S1E, and S1F). At postnatal stage, the mesenchymal/stromal population was highly enriched for *PDGFRA*, a marker for fibro-adipogenic progenitors (FAPs) found in adult mouse SkM (Joe et al., 2010; Uezumi et al., 2010) (Figures 1G, 1H, 1O, 1P, S1G, and S1H). Other cell types present at various levels across limb development include dermal fibroblasts and progenitors (Dermal; *TWIST2*+), Schwann cells (*CDH19*+), smooth muscle cells (SMCs; *MYLK*+), and tenogenic cells (Teno; *TNMD*+). Skin cells (*KRT19*+), endothelial cells (ECs; *ESAM*+), and the hematopoietic (Hema; *SRGN*+) lineages including red blood cells (RBCs) and white blood cells (WBCs) (*HEMGN*+ and *AIF1*+, respectively) were detected at early stages (weeks 5–9) (Figures 1A–1D, 1I–1L, and S1A–S1D), and only residuals of these cell types were found at later stages (week 12 and later), as they were either removed during tissue dissection (skin) or depleted during cell sorting (EC and Hema). In summary, using our scRNA-seq pipeline, we were able to identify dynamic cell populations of both myogenic and non-myogenic nature across human limb development.

### Skeletal Myogenic Subpopulations Vary throughout Human Development

At embryonic weeks 5–6, the myogenic population in the developing hindlimbs was relatively homogeneous and consisted mainly of *PAX3*+ myogenic progenitors (MPs) (Figure 2A). Later,

Figure 1. ScRNA-Seq Identifies Dynamic Cell Types across Human Limb Development

(A–H) Left panels: single cells from human biological replicates grouped by age on t-distributed stochastic neighbor embedding (tSNE) plots and colored by cell type. Right panels: tSNE plots showing color-scaled Muscle.Score (purple to gray, high to low expression). SkM populations are circled in red. (A) Whole hindlimbs of embryonic weeks 5–6. (B) Whole hindlimbs of embryonic weeks 6–7. (C) Whole hindlimbs of embryonic weeks 7–8. (D) Whole hindlimbs of fetal week 9. (E) lineage-depleted hindlimb skeletal muscle tissues of fetal weeks 12–14. (F) Lineage-depleted hindlimb skeletal muscle tissues of fetal weeks 17–18. (G) Lineage-depleted gastrocnemius and quadriceps of juvenile years 7–11. (H) Lineage-depleted quadriceps of adult years 34–42.

(I–P) Bar plots of cell type distribution in biological replicates within age groups. Sample sources and ages in (I–P) correspond to (A–H), respectively, as described above.

See also Figure S1.
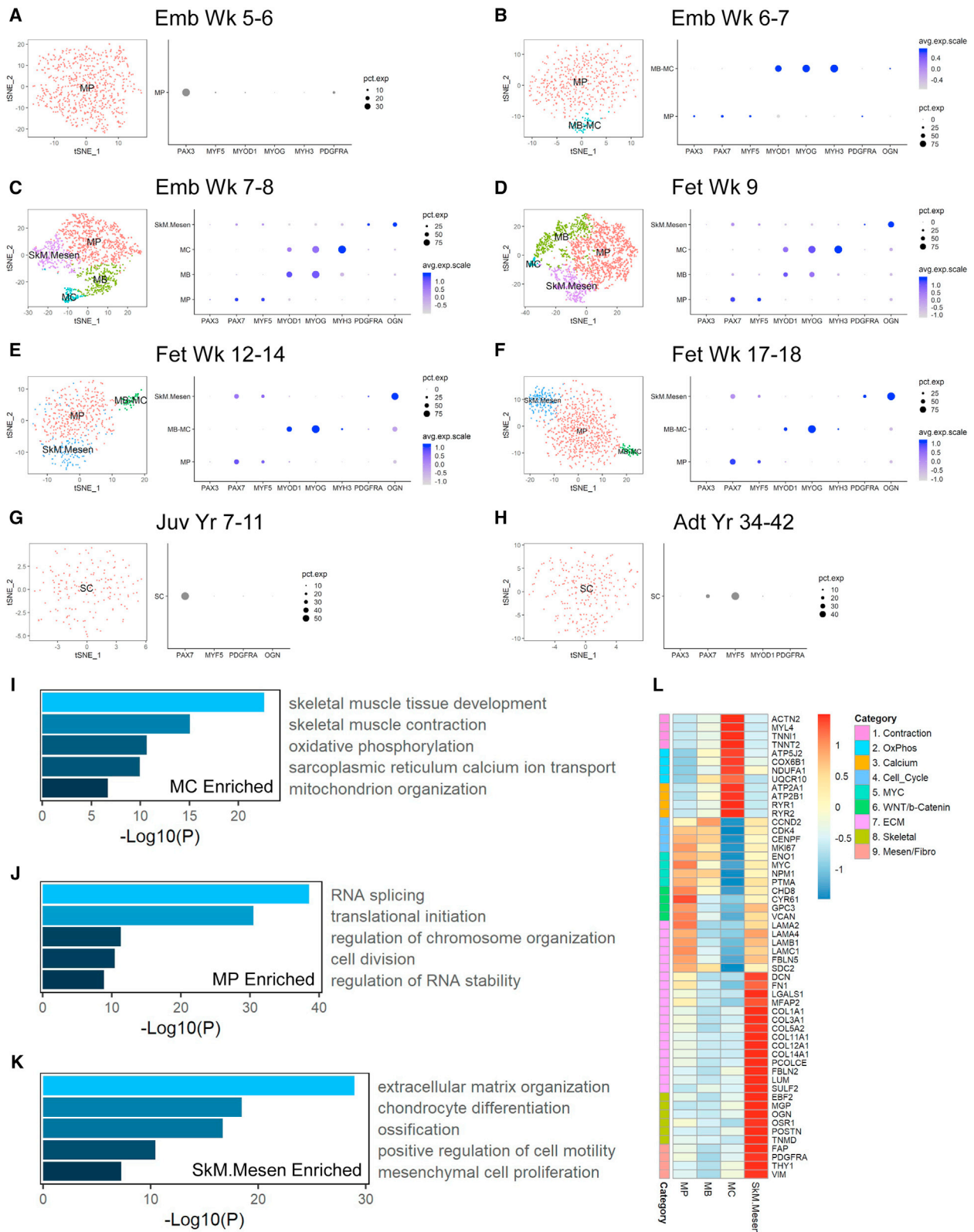
at weeks 6–7, a small subset of differentiating myoblasts-myocytes (MBs-MCs) were observed that expressed commitment and terminal differentiation markers, including *MYOD1*, *MYOG*, and *MYH3* (Figure 2B). At the same time, MPs increased *PAX7* while decreasing *PAX3* expression. The differentiating MB and MC subpopulations became more prominent during weeks 7–9 (Figures 2C and 2D), consistent with the rapid expansion of SkM needed to support prenatal growth. During fetal weeks 12–18, we found reductions of MBs and MCs (Figures 2E and 2F), possibly due to incorporation of most differentiated myogenic cells into multi-nucleated myofibers. At postnatal stage, SkM cells were composed mainly of $PAX7^+$ SCs, with little to no differentiating cells detected (Figures 2G and 2H).

In addition to the myogenic subpopulations reflecting distinct differentiation status, we also found another subpopulation transiently present between weeks 7 and 18. This subset expressed the canonical myogenic markers, albeit at slightly lower levels. Compared with the main myogenic subpopulations (MPs, MBs, and MCs), these cells uniquely expressed genes suggesting a more mesenchymal-like nature, such as *PDGFRA* and *OGN*, and we termed them SkM mesenchymal subtype (SkM.Mesen) (Figures 2C–2F).

To better understand the molecular differences among myogenic subpopulations, we focused on fetal week 9 as an example, as all four subpopulations were readily detected at this time point. We performed differential gene expression of the subpopulations (Table S2), followed by Gene Ontology (GO) analysis as well as gene set enrichment analysis (GSEA). As expected, MCs were enriched for muscle contraction genes compared with MPs. Moreover, MCs highly expressed genes involved in mitochondria and oxidative phosphorylation (OxPhos) as well as calcium signaling (Figures 2I, 2L, and S2A). Proliferating MPs were enriched for genes regulating cell cycle progression, RNA splicing, and protein translation (Figures 2J and 2L). MYC and WNT/β-catenin pathways were also enriched in MPs compared with MCs (Figures 2L and S2B). Another major category of genes enriched in MPs was the extracellular matrix (ECM), which included several members of the laminin family (Figures 2L and S2B). Interestingly, compared with the main myogenic subpopulations, SkM.Mesen cells were also highly enriched for ECM genes, including collagens and regulators of collagen biosynthesis (Figures 2K, 2L, and S2C). To rule out the possibility that the SkM.Mesen subtype was an artifact of misclassification of mesenchymal or skeletogenic cells into the myogenic population by using Seurat (Butler et al., 2018), we used Monocle (Cao et al., 2019), another commonly used scRNA-seq analysis package, to independently confirm this population and found that the vast majority of SkM.Mesen cells were co-clustered with the main SkM subpopulations (Fig-

ure S2D). Although SkM.Mesen cells expressed some pro-chondrogenic genes, such as *COL11A1* and *OGN*, they barely expressed the core chondrogenic determination genes, such as *SOX9* and *COL2A1*, compared with the Chondro population (Figure S2E). Moreover, SkM.Mesen cells in general expressed higher levels of mesenchymal/fibroblastic markers (e.g., *PDGFRA*, *DCN*, *COL3A1*) than the main myogenic subpopulations, but lower than the mesenchymal cell types (Limb.Mesen or PreChondro) (Figure S2E).

To better characterize SkM.Mesen cells, we first performed immunohistochemistry (IHC) staining of PAX7, along with PDGFRA, which is enriched in the SkM.Mesen subpopulation (Figures 2C–2F). We found in human embryonic and fetal limb sections that a subset of PAX7-expressing myogenic cells were co-stained with PDGFRA (Figures 3A and 3B), corroborating the presence of this myogenic subpopulation *in vivo*. To further explore myogenic subpopulations, we examined cell surface markers enriched in the SkM lineage over other cell types and identified CDH15 as a potential surface marker to isolate the total SkM population from human embryonic and fetal limbs (Figure 3C). Next, we performed flow cytometry analysis of CDH15 and PDGFRA (Figure 3D) and sorted cell fractions on the basis of these two markers. In freshly sorted cells, myogenic genes *PAX7*, *MYOD1*, and *MYOG* were upregulated in both $CDH15^+$ fractions compared with the $CDH15^-$ ones, which validated the use of this marker for enriching the total myogenic cells. Interestingly, compared with the $CDH15^+PDGFRA^-$ (15^+P^-) cells, the $CDH15^+PDGFRA^+$ (15^+P^+) cells showed lower expression of myogenic genes but higher expression of genes involved in osteogenesis (*RUNX2* and *COL1A1*) as well as mesenchyme and ECM (*PDGFRA*, *OGN*, and *DCN*) (Figure 3E). When subjected to myogenic and osteogenic differentiation *in vitro*, respectively, 15^+P^- cells showed more prevalent formation of $MyHC^+$ myotubes and higher expression of terminal myogenic differentiation genes (Figures 3F and 3G), while 15^+P^+ cells displayed increased Alizarin red S-stained calcium depots and higher expression of osteogenic differentiation markers (Figures 3H and 3I). By focusing on SkM cells in the developing human hindlimbs, we were able to detect myogenic subpopulations representing not only various commitment status but also unique myogenic/osteogenic bipotential differentiation properties.

Skeletal Muscle Progenitor and Stem Cells at Distinct Stages of Human Development Exhibit Different Gene Expression Programs

We next isolated SMPCs (only the MP subpopulations from prenatal samples) and SCs (from postnatal samples) *in silico* and subjected them to trajectory analysis. These cells formed a developmental trajectory in the diffusion map (DM) space

---

Figure 2. Different Skeletal Myogenic Subpopulations Are Present across Human Development

(A–H) Left panels: single cells classified as "SkM" within each age group on tSNE plots and colored by myogenic subtype. Right panels: dot plots of selected subtype markers. The SkM cells were subsets from total tissue single-cell datasets from (A) embryonic weeks 5–6, (B) embryonic weeks 6–7, (C) embryonic weeks 7–8, (D) fetal week 9, (E) fetal weeks 12–14, (F) fetal weeks 17–18, (G) juvenile years 7–11, and (H) adult years 34–42.

(I–K) Selected enriched GO terms from DEGs enriched in MC versus MP (I), MP versus MC (J), or SkM.Mesen versus the main SkM subpopulations (MP, MB, and MC) (K).

(L) Heatmap of selected markers of different pathways across averaged SkM subpopulations.
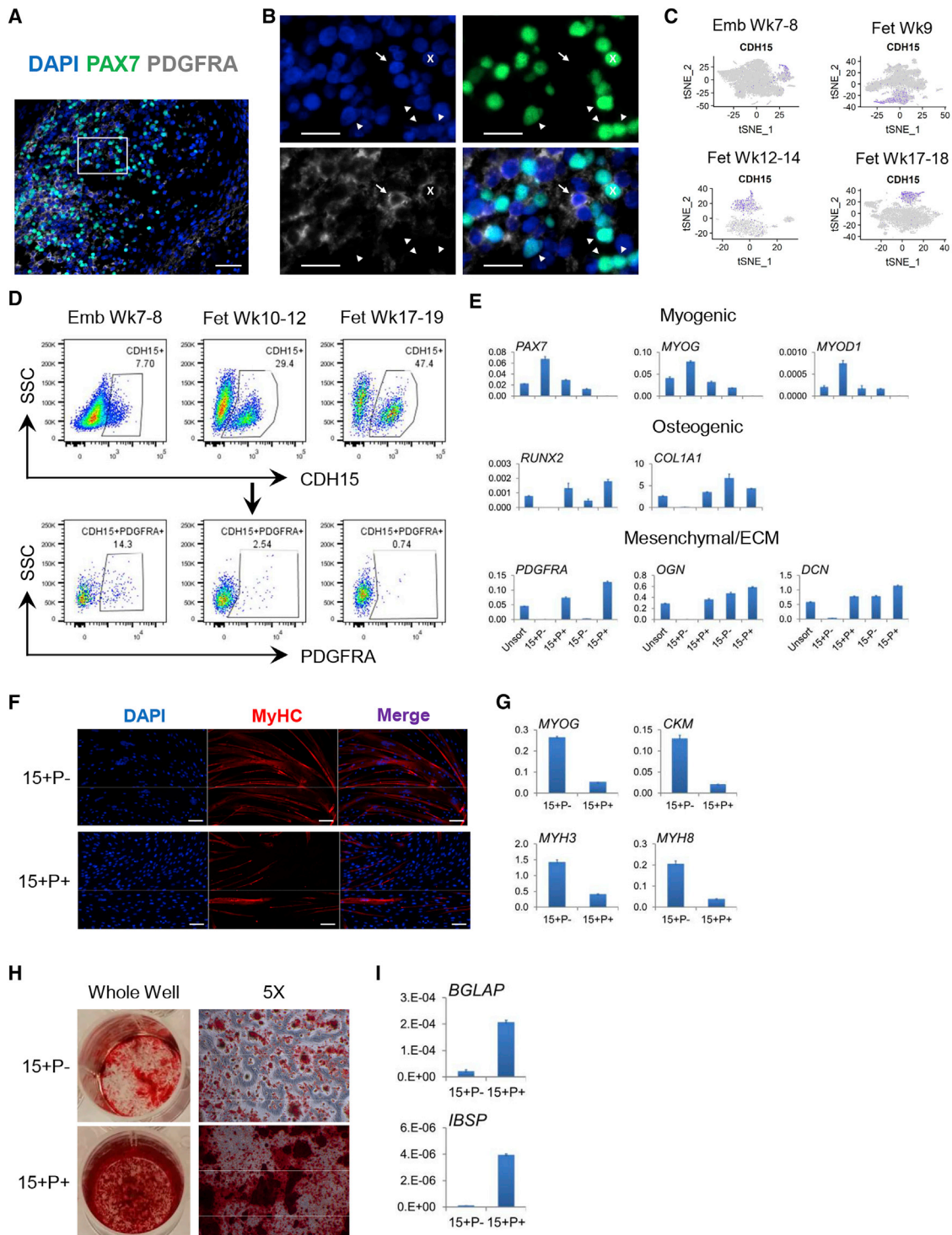
See also Figure S2.

Figure 3. Prospective Isolation and *In Vitro* Differentiation Potential of the SkM.Mesen Subpopulation in Human Embryonic and Fetal Limbs
(A and B) IHC staining of PAX7 and PDGFRA in human limb sections. Images in (B) show enlarged area of the boxed region in (A). Cross (x), PAX7⁺PDGFRA⁺; arrow, PAX7⁻PDGFRA⁺; arrowhead, PAX7⁺PDGFRA⁻. Scale bars represent 50 (A) or 20 (B) μm. Representative images are shown from four week 7–17 human embryonic and fetal limbs.
(C) tSNE plots of CDH15 (purple to gray, high to low expression).
(D) Flow cytometry analysis of CDH15 and PDGFRA co-expression. Representative fluorescence-activated cell sorting (FACS) plots are shown from three or four samples for each age group.

(legend continued on next page)

(Haghverdi et al., 2015) consistent with the ages of individual human samples. Unbiased clustering divided the trajectory into five major stages (Figures 4A, 4B, and S3A). Stage 1 consisted mainly of week 5–6 early embryonic SMPCs, while stage 2 harbored the majority of cells beyond embryonic week 6 to early week 7. Late week 7–8 embryonic SMPCs and those from week 9 in fetal development distributed relatively equally between stages 2 and 3. During fetal development of weeks 12–18, cells gradually progressed from stage 3 to 4. We observed some degree of overlap among sample ages and computationally calculated "stages," suggesting that early prenatal myogenic development is a continuous process. Postnatal SCs from both juvenile and adult muscles constituted stage 5, and they diverged from the prenatal SMPCs on a separate trajectory (Figures 4A, 4B, and S3A).

Although SMPCs and SCs share some common molecular markers and functionalities (Sacco et al., 2008; Tierney et al., 2016), our developmental trajectory analysis indicates that they display significant differences at the transcriptomic level. To further investigate this, we examined differentially expressed genes (DEGs) among distinct stages (Table S3) and found multiple biological processes and pathways differentially regulated across development. Postnatal SCs were enriched for P53 pathway components (Figure 4C) while expressing virtually no cell cycle promoting genes (Figure 4D), consistent with their quiescent state in homeostatic SkM tissues (Flamini et al., 2018). Nevertheless, several growth factor/cytokine signaling genes were enriched in SCs (Figure 4E), suggesting that SCs use specific pathways to actively maintain their quiescence (Price et al., 2014; Shea et al., 2010; Tierney et al., 2014). Two other major differentially regulated biological processes were ECM and cellular metabolism (Figures 4F and 4G). Multiple ECM components showed dynamic expression patterns, including collagens and laminins (Figure 4F). For example, while COL2A1 was uniquely enriched in early embryonic SMPCs (stage 1), COL5A1 gradually increased up to later fetal period (stage 4) and was virtually undetectable at postnatal stage 5. Interestingly, genes facilitating major cellular metabolic pathways (e.g., glycolysis, TCA cycle, OxPhos) were progressively downregulated from early to late developmental stages, while metabolic inhibitors such as TXNIP and PDK4 were increased (Figure 4G). Other dynamically expressed gene sets included mesenchymal-like markers, myogenic cell surface molecules, and Notch signaling components (Figures 4H–4J). Interestingly, genes encoding the major components of the dystrophin-glycoprotein complex (DGC), including dystrophin, dystroglycan, and sarcoglycans, were increased along prenatal development, with the highest expression at fetal weeks 17–18, and then decreased postnatally (Figure 4K).

When examining the canonical TFs involved in myogenesis, we also found distinct expression patterns at each developmental stage (Figure 4L). EYA1, SIX1, and PITX2 showed gradu-ally decreased expression as development progresses. PAX3 progressively decreased while PAX7 increased along development. To corroborate our in silico findings, we performed IHC staining of PAX3 and PAX7 proteins. At week 6, developing human hindlimbs contain only PAX3⁺ and not PAX7⁺ SMPCs, and no MyHC⁺ myofibers could be detected (Figure S3B). At week 7, both PAX3 and PAX7 were detected in limbs, with the proximal region containing PAX7 single-positive cells and the distal region harboring SMPCs transitioning from PAX3 to PAX7 expression. At this stage, thin myofibers were present with single or a small number of myonuclei (Figure S3C). In later fetal and adult stage muscles examined (quadriceps), myofibers continued to grow in size, and SMPCs and SCs were exclusively PAX7⁺ (Figures S3D and S3E). These results confirmed the findings of PAX3 and PAX7 transcript changes across development from our scRNA-seq analysis.

To explore the common features distinguishing between postnatal SCs and prenatal SMPCs, we performed differential gene expression analysis comparing stage 5 SCs with each individual stage SMPCs from stages 1–4 (Table S3). We intersected the upregulated genes in stage 5 SCs from each of the above comparisons and generated a list of 140 genes commonly enriched in SCs compared with SMPCs (Figure 3M). GO analysis showed that several biological processes and signaling pathways were significantly overrepresented, including metabolic and nutrient regulation, intracellular trafficking, ECM organization, and cell adhesion as well as FOXO-mediated cell cycle regulation (Figure 3N). Interestingly, FOXO3 has been shown to promote quiescence of adult SCs in mice (Gopinath et al., 2014), suggesting that the FOXO family and related signaling pathways might play an important role in regulating the transition of proliferative prenatal SMPCs to quiescent postnatal SCs.

Although we have identified CDH15 as a cell surface marker capable of isolating SkM cells from embryonic week 7 to fetal week 19 human limbs, this marker was not shown in our scRNA-seq dataset to be enriched in the myogenic population in embryonic week 5–6 limb tissues (Figure S4F), and no prospective markers for myogenic cell isolation have been established for this developmental stage. Thus, we performed differential gene expression analysis between myogenic and non-myogenic cells and found some known SkM cell surface markers enriched in myogenic versus non-myogenic populations, such as MET and CXCR4 (Bareja et al., 2014; Yin et al., 2013). However, other markers were not expressed at this stage (e.g., CD82) (Alexander et al., 2016; Uezumi et al., 2016) or not distinguishing between myogenic and other cells (e.g., NCAM1 and ITGB1) (Figure S3G) (Castiglioni et al., 2014; Xu et al., 2015). Next, we examined co-expression of PAX3 and MET proteins in week 5–6 human limbs using IHC (Figure S3H). We found nearly overlapping expression patterns of these two proteins at the ventral or dorsal level, but there was a condensed population of PAX3⁻ cells expressing low levels of MET across a small length at the

---

(E) Freshly sorted CDH15 (15) and PDGFRA (P) subpopulations were subjected to qRT-PCR for myogenic, osteogenic, and mesenchymal and ECM gene expression.

(F–I) Sorted 15+P− and 15+P+ cells subjected to myotube fusion followed by IF of MyHC (F) and qRT-PCR of myogenic commitment genes (G) or osteogenic conditions followed by Alizarin red S staining (H) and qRT-PCR of osteogenic differentiation markers (I). Scale bars in (F) represent 100 μm.

Data shown in (E)–(I) are representative of two or three human fetal limbs. Data from qRT-PCR are normalized to RPL13A as mean + SD of technical triplicates. See also Figure S2.
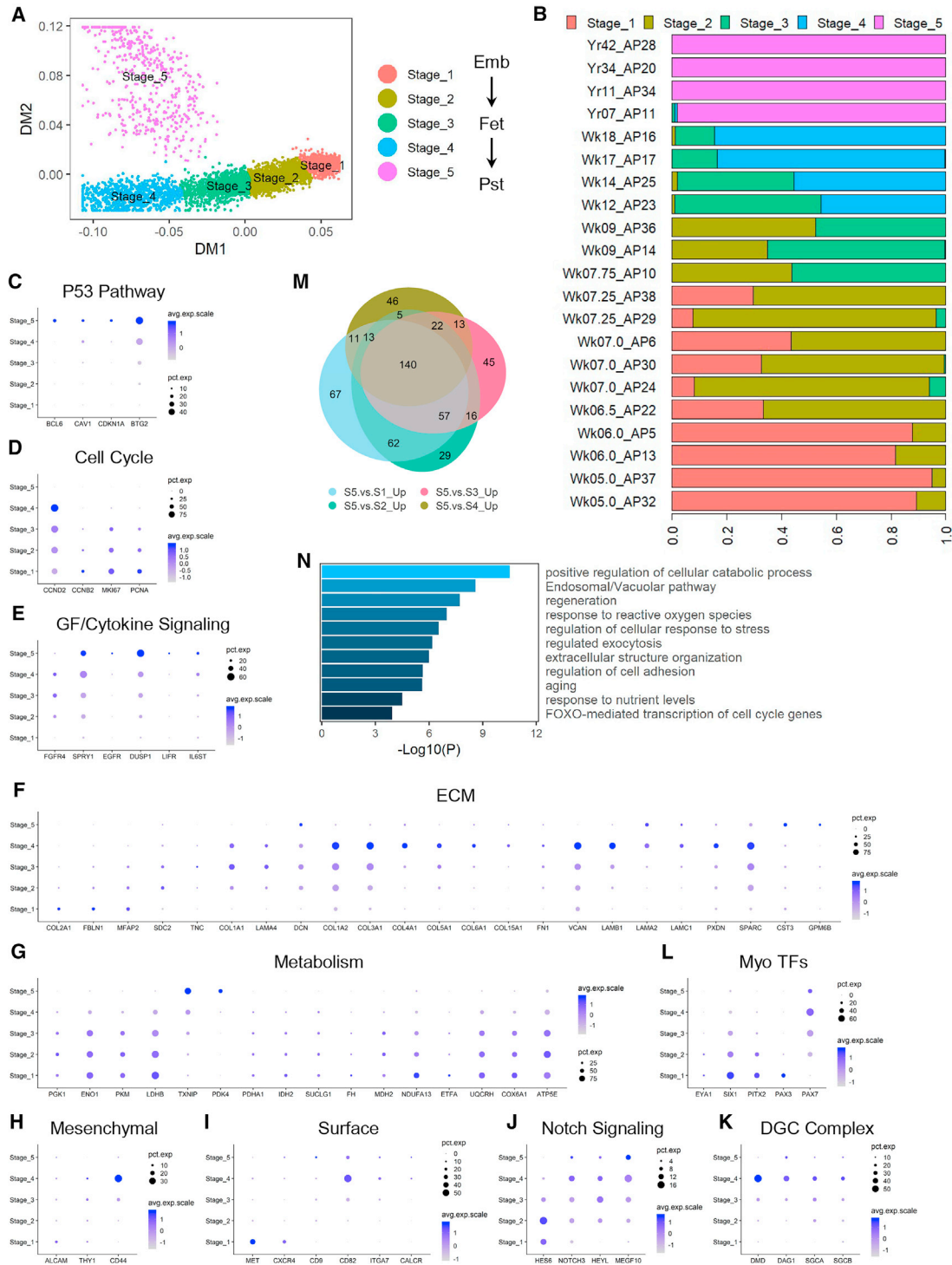
Figure 4. Skeletal Myogenic Progenitor and Stem Cells Display Dynamic Gene Expression Signatures across Human Development

(A) DM plot of single cells of *in vivo* SMPCs and SCs computationally clustered into five major stages.

(B) Proportions of cells from each biological sample assigned to each computational stage.

(C–L) Dot plots of selected genes involved in the P53 pathway (C), the cell cycle (D), growth factor and cytokine signaling (E), extracellular matrix (F), cellular metabolism (G), mesenchymal properties (H), cell surface localization (I), Notch signaling (J), the dystrophin-glycoprotein complex (K), and conventional myogenic transcription factors (L). Pst, postnatal (including juvenile and adult).

(M) Venn diagram of upregulated genes in stage 5 SCs compared with each stage of SMPCs from stages 1–4.

(N) Selected enriched pathways from the 140 genes (M) commonly upregulated in SCs compared with each stage of SMPCs.

See also Figure S3.
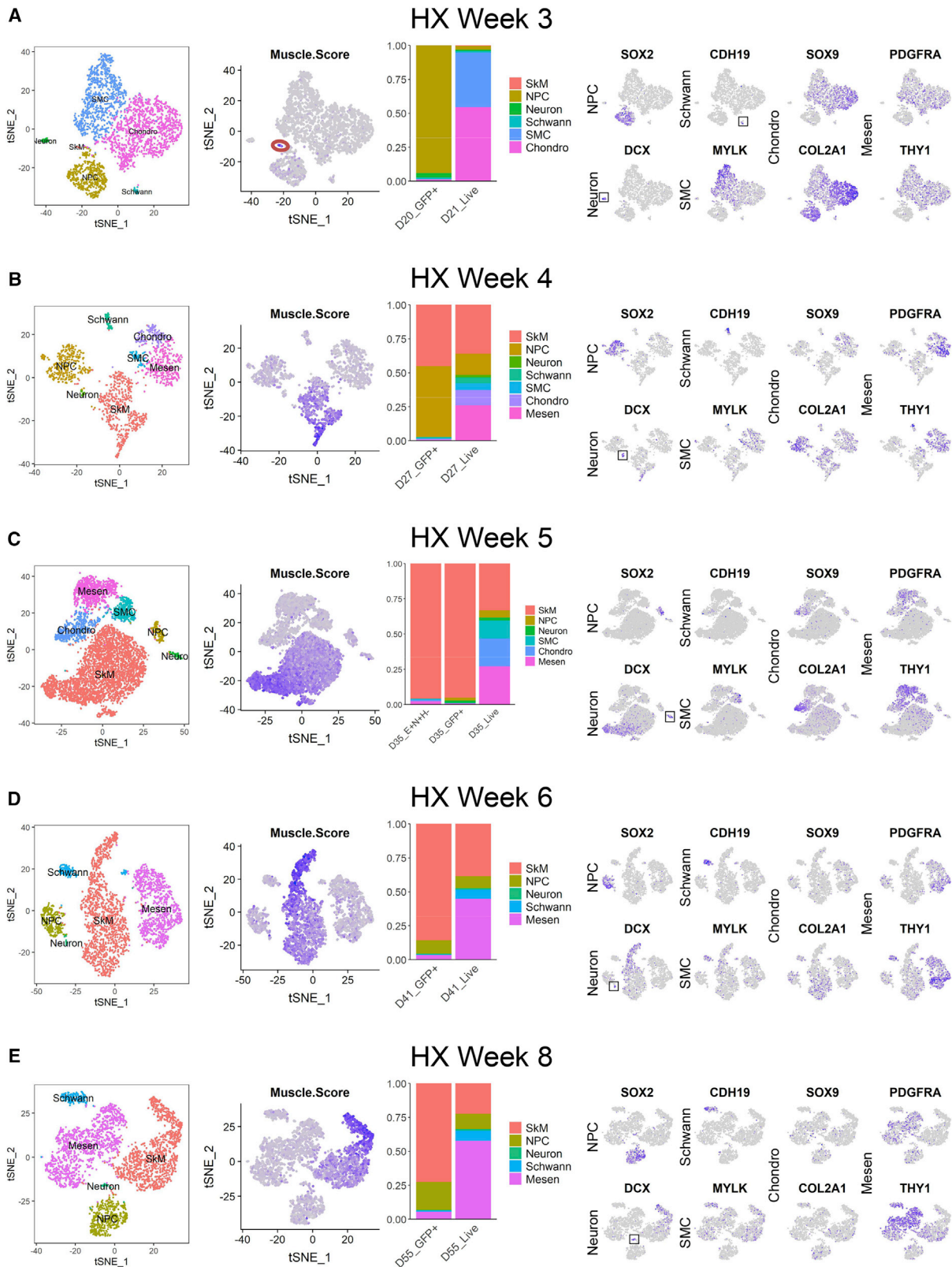
(legend on next page)

central level. When co-stained with CDH2 (Hayashi and Ozawa, 1995; Yajima et al., 1999), these central cells were found to be PAX3⁻METˡᵒʷ/⁺CDH2⁻ (Figure S3G, right panel mosaic images). Thus, we used MET and CDH2 to sort cells from human week 5–6 limbs (Figure S3I) and found the MET⁺CDH2⁺ (M⁺C⁺) fractions highly enriched for *PAX3* and *LBX1* transcripts compared with the MET⁻ fractions or unsorted cells (Figure S3J). When cultured *in vitro*, only M⁺C⁺ cells were supported by the myogenic growth medium and expressed PAX3 proteins, and they could form MyHC⁺ myotubes after switching to fusion conditions (Figure S3K).

Taken together, we mapped SMPCs and SCs from different *in vivo* stage human samples onto a developmental trajectory and unequivocally demonstrated the highly dynamic gene expression profiles of these cells across development. We showed striking differences in expression of genes regulating cellular processes, including ECM and metabolism, and confirmed the observed *in silico* differences of the classical PAX3 and PAX7 myogenic TFs at the protein levels in human tissues. We also identified cell surface markers that enabled prospective isolation of the earliest *PAX3*⁺ myogenic population from week 5–6 developing human limbs.

Directed Myogenic Differentiation of hPSCs Generates Heterogeneous Cell Types Including Both Myogenic and Non-myogenic Cells

Although there are numerous reports describing generation of SkM cells from hPSCs, there is often a large variation in efficiency and consistency in directed differentiation protocols (Kim et al., 2017). We reasoned that by using scRNA-seq, we could identify the different cell types present across representative protocols (see STAR Methods; Table S4). The balance of myogenic and non-myogenic populations may modulate the effectiveness of each differentiation toward SMPCs or SC-like cells. Using our recently published protocol (termed the HX protocol) (Xi et al., 2017), we differentiated hPSCs toward the SkM lineage and profiled all live mononuclear cells in culture from 3–8 weeks of differentiation. To better track PAX7⁺ cells during differentiation, we used CRISPR-Cas9-directed homologous recombination to construct an endogenous *PAX7*-driven GFP reporter in hPSC cell lines (Figures S4A and S4B). These reporter cells were validated to enrich for PAX7 when GFP⁺ cells were sorted after artificial activation of the *PAX7* locus by the dCas9-VPR system (Figures S4C–S4E) or from directed myogenic differentiation (Figures S4F–S4I).

At week 3, the earliest differentiation time point examined, we detected very few SkM cells in dissociated and live-sorted cultures by our scRNA-seq approach. When the reporter cells were used to enrich for PAX7-GFP⁺ cells at this time point, the sorted populations consisted mainly of the neural lineage, including neural progenitor cells (NPCs; *SOX2*⁺) and differenti-ated neurons (*DCX*⁺), while no skeletal myogenic cells could be detected (Figure 5A). Interestingly, the proportion of SkM cells dramatically increased 1 week later at week 4 in live-sorted populations. At the same time, SkM cells increased to close to half of the PAX7-GFP⁺-sorted populations, which was accompanied by a significant decrease in the proportion of neural cells (Figures 5B and S5C). During weeks 5–6 of differentiation, the proportions of SkM cells in live-sorted populations were relatively stable, and they represented the major cell type in PAX7-GFP⁺-sorted populations (Figures 5C, 5D, and S5C). The SkM cell proportions at week 8 of differentiation were slightly decreased in both live- and PAX7-GFP⁺-sorted populations (Figures 5E and S5C). Our scRNA-seq approach also confirmed the enrichment of SkM cells by using a combination of surface markers recently published by our group (Hicks et al., 2018) (Figure 5C).

In addition to SkM and neural cells, we also found multiple other cell types dynamically present in live-sorted populations during the course of differentiation. At week 3 of differentiation, we saw a large portion of chondrogenic cells (*SOX9*⁺/*COL2A1*⁺) and SMCs (*MYLK*⁺) dominating the cultures (Figure 5A), and these populations decreased over time and were absent at 6–8 week time points (Figures 5D and 5E). Meanwhile, a mesenchymal population expressing high levels of *PDGFRA* and *THY1* but not the chondrogenic markers *SOX9* or *COL2A1* arose at week 4 and increased in proportion toward later time points of differentiation (Figures 5B–5E). Another small but persistent cell type seen during the course of directed differentiation (except week 5) was the Schwann cell population (*CDH19*⁺) (Figures 5A, 5B, 5D, and 5E).

Using our scRNA-seq strategy, we also examined the directed myogenic differentiation cultures from two additional protocols widely used by our lab and others published by Chal et al. (2015) and Shelton et al. (2014) (here termed the JC and MS protocols, respectively). At week 5 of differentiation by the JC protocol, we observed both myogenic and non-myogenic populations present in cultures (Figure S5A). The latter included NPCs, neurons, Schwann cells, and a mesenchymal population expressing high levels of *PDGFRA*, *THY1*, and *DCN*, which is likely composed of subpopulations indicated by varying degrees of expression of additional markers (e.g., *ALCAM*, *LUM*, and *COL11A1*). The cellular composition of the differentiation culture at weeks 6–7 using the MS protocol were found to be quite different from that obtained from the HX and JC protocols (Figure S5B). In addition to SkM cells, we observed a robust population highly expressing genes encoding cytokeratins (e.g., *KRT19*) or those pertaining to keratinization (e.g., *PERP*) and therefore is likely involved in epithelium development. There was another major population enriched for genes involved in skeletal development (e.g., *COL1A1* and *OGN*) but lacking strong expression of the canonical commitment markers for the osteogenic, chondrogenic, or tenogenic lineages. We also

Figure 5. ScRNA-Seq Identifies Skeletal Myogenic Populations as Well as Other Cell Types during hPSC Differentiation
(A–E) Single-cell analysis on hPSC-derived samples using the HX protocol grouped by differentiation time at 3 weeks (A), 4 weeks (B), 5 weeks (C), 6 weeks (D), and 8 weeks (E). From left to right: first panels: tSNE plots of individual cells colored by cell type. Second panels: tSNE plots showing color-scaled Muscle.Score (purple to gray, high to low expression). The tiny SkM population at week 3 is circled in red. Third panels: bar plots of cell type distribution in enriched or un-enriched samples at similar differentiation time points. Fourth panels: tSNE plots of selected cell type markers (purple to gray, high to low expression). Small populations are boxed for easy visualization.
See also Figures S4 and S5.
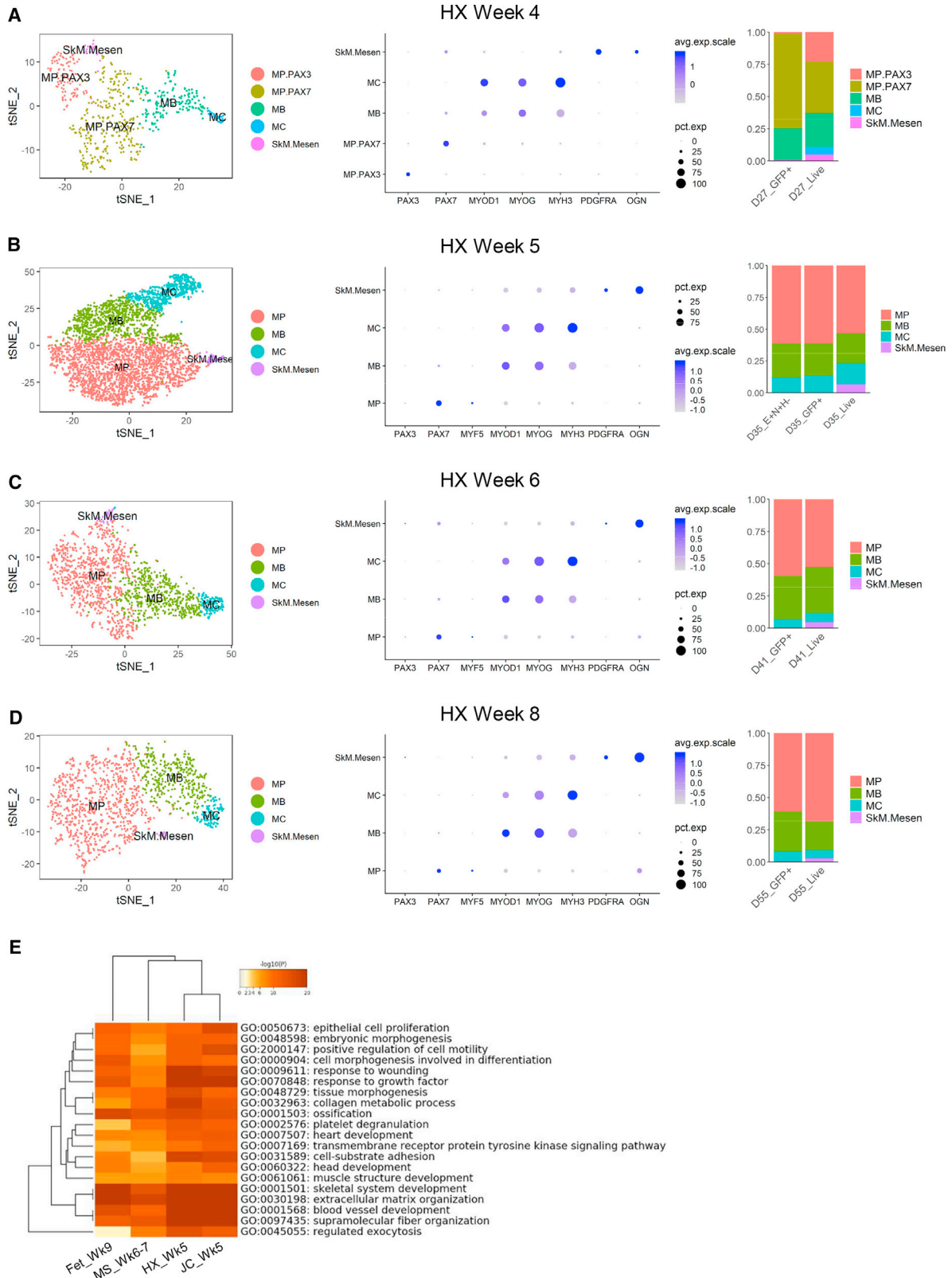
(legend on next page)

found a small subset of cells enriched for genes participating in cholesterol biosynthesis (*CRABP1* and *CRABP2*), but the accurate identity of this population is yet to be determined.

In conclusion, our scRNA-seq approach identified dynamic cellular compositions, both myogenic and non-myogenic, during the course of hPSC SkM-directed differentiation across multiple protocols. This provides a unique resource to not only further explore hPSC-derived myogenic cells, but also other cell types present in the differentiation cultures and their potential influences on *in vitro* hPSC myogenesis.

Skeletal Muscle Cells Derived *In Vitro* from hPSCs Harbor Multiple Myogenic Subpopulations during the Course of Directed Differentiation

Similar to our approach on studying *in vivo* human myogenesis, we bioinformatically isolated the SkM cells from cultures examined during 4–8 weeks of *in vitro* hPSC-directed differentiation using the HX protocol. Consistent with our *in vivo* findings, we also found subpopulations representing different myogenic commitment status (i.e., MP, MB, and MC cells at all time points of directed differentiation), and the relative distribution of these three subpopulations largely stayed constant regardless of differentiation timing or enrichment strategies (Figures 6A–6D). Of note, we detected MBs and MCs within the SkM populations even from PAX7-GFP⁺-sorted fractions. This is likely due to the low expression of *PAX7* in early committed MBs (Figures 6A–6D, middle panels) and the high stability of the GFP proteins (Li et al., 1998) retained in committed cells that have previously expressed *PAX7*. Interestingly, MPs at 4 weeks of directed differentiation from live-sorted populations could be further subdivided into two subsets, enriching for *PAX3* and *PAX7*, respectively. As expected, MPs at this differentiation time point from PAX7-GFP⁺-sorted SkM cells were composed mainly of *PAX7*⁺, with only barely detectable *PAX3*⁺ progenitors (Figure 6A). However, at later time points, MPs from either live- or PAX7-GFP⁺-sorted fractions did not show obvious expression of *PAX3* and expressed only *PAX7* (Figures 6B–6D). This is similar to the *PAX3*-to-*PAX7* transition that we observed at early *in vivo* human limb myogenesis (Figures 2A–2H, 4L, and S3B–S3E). Reminiscent of the SkM.Mesen subpopulation found during weeks 7–18 of prenatal development (Figures 2C–2F), we observed a small but consistent "side" population in all examined directed differentiation time points (we also termed these cells "SkM.Mesen" but in an *in vitro* context). This subset of cells showed slightly higher expression of myogenic activation and commitment markers *MYOD1*, *MYOG*, and *MYH3* than MPs, but much lower than MBs and MCs, suggesting that they are not fully committed terminally differentiated muscle cells. Meanwhile, they showed appreciably lower expression of the stem/progenitor marker *PAX7* than MPs, and indeed this subpopulation was detectable only

in live-sorted but not PAX7-GFP⁺-enriched cell fractions (Figures 6A–6D).

When examining the SkM subpopulations from the JC and MS protocols, we found similar MP, MB, and MC subsets, though their relative proportions varied across different protocols (Figures S5D and S5E). Again, we observed the SkM.Mesen subpopulations from both protocols that share many of the enriched genes and biological processes with similar populations from the HX protocol as well as *in vivo* week 9 fetal samples (Figures 6E and S5F; Table S2).

Here, we consistently identified, across multiple hPSC myogenic differentiation protocols, major and rare subpopulations within the SkM cells. This allows us to better understand the dynamics of myogenic lineage development modeled *in vitro* by hPSCs.

hPSC-SMPCs Generated from Multiple Protocols Align to a Developmental Stage of Late Embryonic to Early Fetal Transition

To determine the molecular identity of hPSC-derived SMPCs, we mapped the MP subpopulations from all differentiation time points generated from the HX protocol along with the *in vivo* progenitor and stem cells on DM space. The *in vivo* cells largely retain their developmental trajectory from stages 1 to 5, as previously analyzed (Figure 4A), with minor changes possibly due to variations introduced by adding in the *in vitro* cells. SMPCs derived from hPSCs aligned to the stage 2 and 3 *in vivo* SMPCs along the DM1 component and diverged along DM2, which likely results from culture-related effects (Figures 7A and 7B). To more quantitatively assess the developmental timing of the cells, we developed a more linear method to calculate each cell's developmental score (Dev.Score), in which we took into account the expression levels of postnatal versus embryonic enriched genes in individual cells (see STAR Methods). Using this independent method, we again found *in vitro* hPSC-derived SMPCs aligned to *in vivo* SMPCs of stages 2 to 3, which corresponds to the embryonic week 7 to fetal week 12 transition period (Figure 7C). Furthermore, we included additional SMPCs generated from the JC and MS protocols in our analysis pipeline and found that hPSC-SMPCs derived from all protocols mapped to a similar late embryonic to early fetal transition stage of human myogenesis (Figures S6A–S6D).

To further explore the differences underlying the separation of *in vivo* and *in vitro* SMPCs, we compared the gene expression profiles of hPSC-derived MPs from all three protocols with *in vivo* progenitors from stages 2 and 3, a developmental period to which the hPSC-SMPCs most closely align. Hierarchical clustering of these five groups of cells showed major segregation on the basis of source of *in vivo* or *in vitro* derivation, and within the *in vitro* hPSC-SMPCs, those generated from the HX and JC protocols were closer to each other than those from the MS

Figure 6. ScRNA-Seq Identifies Myogenic Subpopulations during hPSC Myogenic Differentiation

(A–D) Single cells classified as "SkM" from cultures derived using the HX protocol grouped at similar time points at 4 weeks (A), 5 weeks (B), 6 weeks (C), and 8 weeks (D) of differentiation. Left panels: tSNE plots of individual cells colored by myogenic subtype. Middle panels: dot plots of selected subtype markers. Right panels: bar plots of subtype distribution in enriched or unenriched samples at similar differentiation time points.

(E) DEGs upregulated in SkM.Mesen versus the main SkM subpopulations (MP, MB, and MC) from three hPSC differentiation protocols as well as human fetal week 9 samples were subjected to GO enrichment analysis. Heatmap clustering of the top 20 shared GO groups on the basis of enrichment p values.
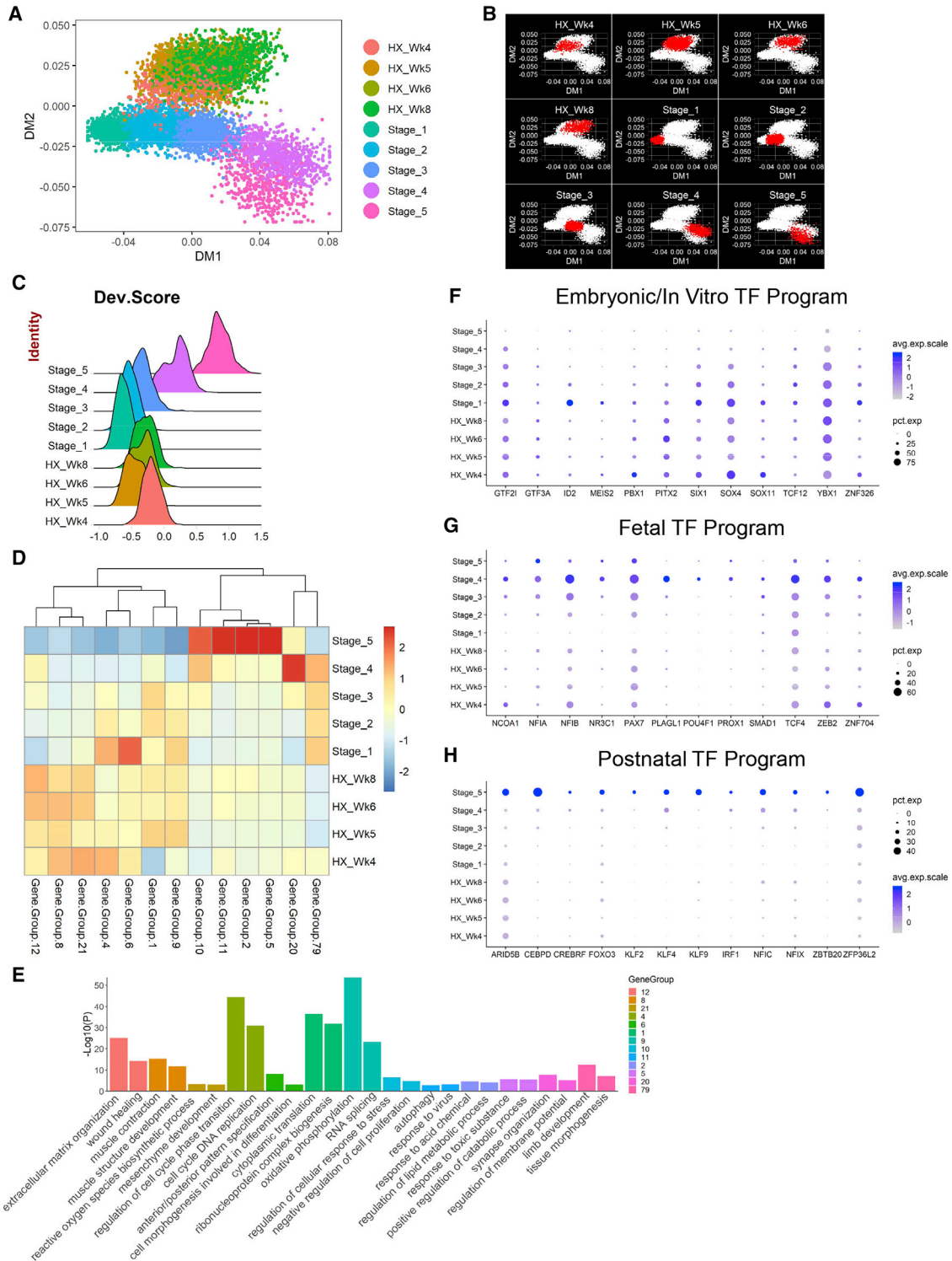
See also Figures S4 and S5.

Figure 7. *In Vitro* hPSC-SMPCs Align to an Embryonic-to-Fetal Transition Stage of *In Vivo* Human Myogenesis
(A) DM plot of single cells of *in vivo* and *in vitro* (HX protocol) SMPCs and SCs.
(B) DM plots highlighting cells (in red) from individual *in vivo* or *in vitro* (HX protocol) stages.
(C) Ridge plot of developmental score (Dev.Score) distribution across *in vivo* or *in vitro* (HX protocol) stages.
(D) Heatmap of selected co-regulated gene groups (gene number > 50) across averaged *in vivo* or *in vitro* (HX protocol) stages.
(E) Two selected enriched GO terms from each gene group are plotted and color-coded.
(F–H) Dot plots of selected TFs differentially enriched in embryonic/*in vitro* (F), fetal (G), and postnatal (H) stages.
See also Figures S6 and S7.

protocol (Figure S6E). Next, we performed differential gene expression analysis between each of the three hPSC-SMPC populations compared with the stage 2 or 3 populations (Table S5) and found genes that are commonly enriched in either *in vivo* stage 2 or 3 cells (Figures S6F and S6G) and vice versa (Figures S6H and S6I). Subsequently, GO analysis of these genes revealed biological processes and signaling pathways consistently upregulated in SMPCs from *in vivo* stages compared with all of the three *in vitro* myogenic protocols. These include both positive (*CCND1* and *CDK6*) and negative (*SPRY1* and *DUSP1*) regulation of cell cycle, indicating more orchestrated cell cycle progression, RNA splicing (*RPS26* and *RBM39*), WNT signaling pathways (*FRZB* and *TCF12*), and SkM development (*MYF5*, *MSTN*, and *VGLL2*) (Figures S6F, S6G, and S6J). On the other hand, processes and pathways consistently enriched in *in vitro*-derived cells from all three protocols include muscle contraction (*MYL1*, *CKB*, and *KLHL41*), cell motility (*NEFL* and *YBX3*), lipid metabolism (*FDFT1*, *NPC2*, and *TSPO*), and ECM (*DCN* and *MGP*) (Figures S6H, S6I, and S6K). These findings suggest that there are fundamental differences between SMPCs derived *in vivo* compared with *in vitro*, although they might represent a similar developmental stage.

To better understand the gene regulatory networks distinguishing the different myogenic stem and progenitor cells arising during *in vivo* human development and derived from hPSC-directed differentiation, we performed gene co-regulation analysis on our scRNA-seq data (see STAR Methods). We found that co-regulated gene groups differentially expressed at distinct stages of myogenesis (Figure 7D; Table S6) and performed GO analysis to explore the key biological processes and pathways enriched in these gene networks (Figure 7E). For example, gene groups 12, 8, and 21 were upregulated in the *in vitro* hPSC-SMPCs compared with the *in vivo* cells, and they were enriched for GO terms such as ECM, muscle contraction, and reactive oxygen species. Cell cycle, translation, energy metabolism, and morphogenesis and patterning were enriched in gene groups upregulated in early embryonic as well as hPSC-SMPCs, such as groups 4, 1, 9, and 6. For gene groups upregulated in postnatal SCs (groups 10, 11, 2, and 5), enriched biological processes were in general involved in maintaining cellular homeostasis. Group 20 was found to be uniquely expressed at high levels in stage 4 SMPCs (fetal weeks 17–18) and was enriched for genes participating in neuromuscular junction establishment. Group 79 was expressed at a relatively stable level across prenatal development, but at low levels in hPSC-SMPCs or postnatal SCs, and this group enriched for processes such as limb morphogenesis. Next, we focused on the TFs within each of the gene groups, as they have been shown to be the master regulators in cell fate decisions in multiple systems (Oh and Jang, 2019). We found distinct TF programs that were differentially enriched in embryonic/*in vitro*, fetal, and postnatal stages (Figures 7F–7H). These TFs included some canonical myogenic factors, such as *PITX2* and *SIX1*, that were enriched in SMPCs from early *in vivo* stages and derived from hPSCs (Figure 7F), which is consistent with our previous findings (Figure 4L). However, most of these TFs are not classic myogenic genes, which indicates that maturation of MP and stem cells involves processes beyond the regulation of myogenic identity. Furthermore, using RNAscope coupled with IHC, we confirmed the dynamic expres-

sion patterns of selected TFs (*NFIX*, *NFIC*, *KLF9*, and *CEBPD*) in PAX7$^+$ SMPCs/SCs in limb tissues from different embryonic, fetal, and adult stages (Figure S7). Overall, these analyses provide potential candidate pathways and TFs to manipulate the maturation status of SMPCs in the future.

DISCUSSION

Myogenesis occurs from early embryonic to postnatal periods and involves myogenic as well as other supportive cell types. Yet myogenic development in human is poorly understood. Although recent work has profiled SkM using scRNA-seq (Barruet et al., 2020; De Micheli et al., 2020; Dell'Orso et al., 2019; Giordani et al., 2019; Rubenstein et al., 2020; Tabula Muris Consortium et al., 2018), the scope was limited to adult tissues. In this work, we provide a comprehensive roadmap of *in vivo* human limb myogenesis at the single-cell level across development from as early as embryonic week 5 up to adulthood. We also interrogated *in vitro* hPSC myogenic differentiation from multiple published protocols. Through trajectory analysis, we showed that MP and stem cells from different developmental stages possess distinct gene expression profiles, and hPSC-derived SMPCs align to an *in vivo* stage of late embryonic to early fetal transition.

One interesting observation is the identification of a resident embryonic and fetal SkM subpopulation that expresses reduced canonical myogenic markers but increased levels of mesenchymal (e.g., *PDGFRA*, *OGN*, *THY1*, and *DCN*) and skeletal lineage genes (e.g., *RUNX2*, *COL1A1*, *MGP*, and *TNMD*) (Figures 2, 3, and S2; Table S2). When isolated and cultured *in vitro*, this SkM.Mesen subpopulation showed weaker myogenic fusion but stronger osteogenic differentiation capacities. These unique cells could represent a transient subset of myogenic cells existing during early myogenic development that have a higher propensity of osteogenic fate adoption. Indeed, it has been shown that human second trimester fetal SkM cells harbor myogenic and osteogenic bipotency when isolated and cultured *in vitro* (Castiglioni et al., 2014; Tanaka et al., 2012). A similar "side" population of SkM.Mesen was also detected from all three hPSC myogenic differentiation protocols (Figures 6 and S5; Table S2). However, whether these *in vitro* SkM.Mesen cells are the same as those detected *in vivo* or a small subset drifting away from their myogenic identity due to culture conditions needs to be further explored. It will also be interesting to fully characterize other cell types during the transition from prenatal to postnatal limb development. Deciphering and co-opting the roles of supportive cells *in vivo* could increase our ability to mature and improve the functional potential of SMPCs derived from hPSCs *in vitro*.

Our scRNA-seq pipeline enabled us to focus on the differences of the progenitor and stem cell subpopulations within the SkM lineage across development, avoiding potential influences such as commitment status from the other myogenic subpopulations. Accordingly, we were able to confidently map the developmental trajectory of SMPCs and SCs across development and identify gene expression differences that distinguishes each of them (Figures 4 and S3).

Striking differences in ECM components have been recently reported in fetal and postnatal mouse MP and stem cells, and

they are critical for the differential regenerative capacities of cells from different developmental stages (Tierney et al., 2016). Here, we also found that ECM gene expression is one of the key features that significantly changed across human development (Figure 4F; Table S3), suggesting ECM remodeling as a critical process in response to both the intrinsic cues and extrinsic cell-cell/cell-matrix interactions during the SMPC-to-SC transition in human development.

Metabolism is becoming a key feature of cell fate regulation in model organisms, including somite specification and mouse SC states (Koopman et al., 2014; Oginuma et al., 2017; Pala et al., 2018; Ryall, 2013; Ryall et al., 2015; Yucel et al., 2019) but has not been carefully evaluated throughout embryonic and fetal to adult development. We found that multiple genes participating in central metabolism were expressed at higher levels in early embryonic SMPCs and gradually decreased as cells transition to postnatal SCs. Consistently, negative metabolic regulators such as *TXNIP*, an inhibitor of glucose uptake and glycolysis and *PDK4*, which downregulates pyruvate entry into the mitochondrial TCA cycle, were found to be upregulated in postnatal SCs (Figure 4G; Table S3). This gene expression pattern most likely reflects the changing metabolic demands as actively expanding SMPCs during prenatal muscle establishment transition to quiescent SCs in postnatal homeostasis, and suggests that metabolic wiring distinguishes SMPC and SC states.

Although there are multiple protocols reporting generation of SkM cells from hPSCs, the heterogeneity and dynamics of cell types present in culture and within the myogenic populations have not been adequately studied. Using scRNA-seq, we undoubtedly found myogenic as well as significant numbers of non-myogenic populations from all three representative protocols examined (Figures 5 and S5). Both the HX and JC protocols involve a sequential specification through presomitic mesoderm, somite, dermomyotome, and SkM, and they yielded similar cell types in the differentiation cultures. Both of these two protocols generated neural cell types, including NPCs, neurons, and Schwann cells. It is worth noting that the WNT activation and BMP and TGF-β inhibition approach used in these protocols have also been used in strategies to differentiate hPSCs toward neural crest (NC) cells (Chambers et al., 2009), which are ancestors of multiple cell types, including peripheral neurons, Schwann cells, SMCs, and craniofacial cartilage and bone, among others (Cheung et al., 2019). Thus, it is conceivable that the neural cell types generated from these protocols might be derived from NC cells that were specified along with somite early on during differentiation. Moreover, in the HX protocol, we observed SMCs and chondrogenic cells present at early time points (weeks 3–4) but with decreased proportions (week 5) and eventually undetectable (weeks 6–8) toward later time points. These populations could be derivatives from either NC or somite cells (Brent and Tabin, 2002), and the decrease of their presence might reflect the unsuitableness of the myogenic conditions to support them in long-term culture. The origin of the mesenchymal populations starting at week 4 will be interesting to explore further and might be derived from a rare population generated early on during differentiation, or from cells not well supported in culture that drift away from their original identities. Future *in vitro* lineage tracing and depletion experiments will be required to delineate the origins of these non-myogenic popula-

tions and their influences on the myogenic specification efficiencies of the protocols.

This resource provides the ability for any lab performing hPSC differentiation to map the developmental identity of MP or stem cells. It is very striking that across all three different protocols, SMPCs derived from hPSCs align comparably to the *in vivo* embryonic-to-fetal transition stage and are not equivalent to the postnatal juvenile and adult SCs (Figure 7; Figure S6). Prolonging the length of directed differentiation (HX protocol; up to 8 weeks) does not seem to drive hPSC-SMPCs beyond this transitioning stage. Of note, even compared with the *in vivo* SMPCs at embryonic-to-fetal transition, hPSC-SMPCs still show fundamental differences in a wide range of biological processes (Figure S6). These suggest that stringent evaluation is required to correctly determine cell identity, molecular property, and functional potential of myogenic derivatives across differentiation strategies from hPSCs.

To better understand the regulatory network underlying myogenic development, we performed gene co-regulation analysis and identified developmental stage-specific gene group signatures. Focusing on TFs within each group, we provide key TF programs that can serve as potential maturation factors for manipulating progenitor and stem cell states across development (Figure 7; Table S6). We found canonical myogenic specification factors such as *SIX1*, *PITX2*, and *PAX7*. We also found other genes known to regulate SkM, such as *ID2* and *TCF12* (Zhao and Hoffman, 2004) that were enriched in the embryonic and hPSC-derived SMPCs, *SMAD1* (BMP signaling) (Sartori and Sandri, 2015) and *PROX1* (Kivelä et al., 2016; Petchey et al., 2014) that were increased from early embryonic to late fetal stage and decreased postnatally, and *FOXO3* (Sanchez et al., 2014) that was specifically expressed at high levels in postnatal SCs. Interestingly, we found all of the nuclear factor I family members (*NFIA*, *NFIB*, *NFIC*, and *NFIX*) expressed at higher levels in late fetal or postnatal stages, suggesting this TF family might play an important role in myogenic maturation. In fact, *NFIX* has been reported to control the switch from embryonic-to-fetal myogenesis in both mouse and zebrafish (Messina et al., 2010; Pistocchi et al., 2013; Taglietti et al., 2018). Moreover, it is worth noting that the majority of the identified network genes are not typical myogenic TFs. For example, the Kruppel-like factor family members *KLF2*, *KLF4*, and *KLF9* were all enriched in postnatal SCs. This family of genes participates in the development and homeostasis of numerous tissues (McConnell and Yang, 2010), and KLF4 is well-known of its ability in induced pluripotency by acting as a pioneer factor that facilitates large-scale chromatin remodeling (Schmidt and Plath, 2012; Takahashi and Yamanaka, 2016). Along this line, we also found other chromatin modifiers differentially expressed across development, including *ARID5B*, *NCOA1*, and *NR3C1*. These observations suggest a model in which concerted efforts from canonical myogenic TFs as well as epigenetic and chromatin regulators are required to shape the gene regulatory landscapes and drive SMPC-to-SC transition during development. This intricate interplay will also likely be required to instruct hPSCs to gain a SC-like state and maintain their cell fate identity in culture.

In summary, this work serves as a resource for advancing our knowledge of human myogenesis. It also provides a tool for molecular identification of hPSC-derived SMPCs and targets to

guide the generation of the most regenerative cells for translational applications in SkM-based regenerative medicine.

STAR★METHODS

Detailed methods are provided in the online version of this paper and include the following:

- KEY RESOURCES TABLE
- RESOURCE AVAILABILITY
  - Lead Contact
  - Materials availability
  - Data and code availability
- EXPERIMENTAL MODEL AND SUBJECT DETAILS
  - Human tissues
  - Cell lines
- METHOD DETAILS
  - Cell preparation for single cell RNA-sequencing
  - Cell capture and library construction for single cell RNA-sequencing
  - Human PSC maintenance
  - Human PSC skeletal myogenic directed differentiation
  - PAX7-GFP reporter cell construction
  - PAX7-GFP reporter validation
  - FACS cell sorting
  - Immunofluorescence
  - Cytospin
  - Immunohistochemistry with tyramide signal amplification
  - RNAscope with Immunohistochemistry
  - Quantitative real time-PCR
  - *In vitro* myotube fusion assay
  - *In vitro* myogenic and osteogenic bipotential differentiation assays
- QUANTIFICATION AND STATISTICAL ANALYSIS
  - Processing, read alignment and digital gene expression matrix generation
  - Computational analysis using Seurat
  - Analysis using Monocle3
  - Gene ontology enrichment analysis
  - Gene set enrichment analysis
  - Co-regulated gene network analysis
  - Hierarchical clustering
  - Gene list intersection and Venn diagram generation

SUPPLEMENTAL INFORMATION

Supplemental Information can be found online at https://doi.org/10.1016/j.stem.2020.04.017.

AUTHOR CONTRIBUTIONS

Conceptualization, H.X., A.D.P., B.V.H., and K.P.; Methodology, H.X., J.L., S.S., and C.S.Y.; Software, H.X., J.L., and S.S.; Data Curation, H.X.; Visualization, H.X.; Project Administration, A.D.P.; Validation, H.X.; Formal Analysis, H.X., J.L., and S.S.; Investigation, H.X., J.L., S.S., P.C., C.S.Y., S.Y., M.H., K.G., W.F., J.M., and S.L.; Resources, A.D.P., K.S.-L., M.S., K.P., and D.E.; Writing – Original Draft, H.X. and A.D.P.; Writing – Review & Editing, H.X., J.L., S.S., P.C., C.S.Y., S.Y., M.H., M.S., B.V.H., D.E., K.S.-L., K.P., and A.D.P.; Supervision, A.D.P. and K.P.; Funding Acquisition, A.D.P.

DECLARATION OF INTERESTS

C.S.Y., M.S., and A.D.P. are co-founders of and have financial interests in MyoGene Bio. The Regents of the University of California have licensed intellectual property invented by C.S.Y., M.S., and A.D.P. to MyoGene Bio. M.S. and A.D.P. serve on the scientific advisory board of MyoGene Bio. C.S.Y. is currently CEO of MyoGene Bio.

REFERENCES

Akiyama, H., Kim, J.E., Nakashima, K., Balmes, G., Iwai, N., Deng, J.M., Zhang, Z., Martin, J.F., Behringer, R.R., Nakamura, T., and de Crombrugghe, B. (2005). Osteo-chondroprogenitor cells are derived from Sox9 expressing precursors. Proc. Natl. Acad. Sci. U S A *102*, 14665–14670.

Alexander, M.S., Rozkalne, A., Colletta, A., Spinazzola, J.M., Johnson, S., Rahimov, F., Meng, H., Lawlor, M.W., Estrella, E., Kunkel, L.M., and Gussoni, E. (2016). CD82 is a marker for prospective isolation of human muscle satellite cells and is linked to muscular dystrophies. Cell Stem Cell *19*, 800–807.

Applebaum, M., and Kalcheim, C. (2015). Mechanisms of myogenic specification and patterning. Results Probl. Cell Differ. *56*, 77–98.

Bareja, A., Holt, J.A., Luo, G., Chang, C., Lin, J., Hinken, A.C., Freudenberg, J.M., Kraus, W.E., Evans, W.J., and Billin, A.N. (2014). Human and mouse skeletal muscle stem cells: convergent and divergent mechanisms of myogenesis. PLoS ONE *9*, e90398.

Barna, M., and Niswander, L. (2007). Visualization of cartilage formation: insight into cellular properties of skeletal progenitors and chondrodysplasia syndromes. Dev. Cell *12*, 931–941.

Barruet, E., Garcia, S.M., Striedinger, K., Wu, J., Lee, S., Byrnes, L., Wong, A., Xuefeng, S., Tamaki, S., Brack, A.S., and Pomerantz, J.H. (2020). Functionally heterogeneous human satellite cells identified by single cell RNA sequencing. eLife *9*, e51576.

Belle, M., Godefroy, D., Dominici, C., Heitz-Marchaland, C., Zelina, P., Hellal, F., Bradke, F., and Chédotal, A. (2014). A simple method for 3D analysis of immunolabeled axonal tracts in a transparent nervous system. Cell Rep. *9*, 1191–1201.

Borchin, B., Chen, J., and Barberi, T. (2013). Derivation and FACS-mediated purification of PAX3+/PAX7+ skeletal muscle precursors from human pluripotent stem cells. Stem Cell Reports 1, 620–631.

Brent, A.E., and Tabin, C.J. (2002). Developmental regulation of somite derivatives: muscle, cartilage and tendon. Curr. Opin. Genet. Dev. 12, 548–557.

Butler, A., Hoffman, P., Smibert, P., Papalexi, E., and Satija, R. (2018). Integrating single-cell transcriptomic data across different conditions, technologies, and species. Nat. Biotechnol. 36, 411–420.

Cao, J., Spielmann, M., Qiu, X., Huang, X., Ibrahim, D.M., Hill, A.J., Zhang, F., Mundlos, S., Christiansen, L., Steemers, F.J., et al. (2019). The single-cell transcriptional landscape of mammalian organogenesis. Nature 566, 496–502.

Castiglioni, A., Hettmer, S., Lynes, M.D., Rao, T.N., Tchessalova, D., Sinha, I., Lee, B.T., Tseng, Y.H., and Wagers, A.J. (2014). Isolation of progenitors that exhibit myogenic/osteogenic bipotency in vitro by fluorescence-activated cell sorting from human fetal muscle. Stem Cell Reports 2, 92–106.

Cerletti, M., Shadrach, J.L., Jurga, S., Sherwood, R., and Wagers, A.J. (2008). Regulation and function of skeletal muscle stem cells. Cold Spring Harb. Symp. Quant. Biol. 73, 317–322.

Chal, J., and Pourquié, O. (2017). Making muscle: skeletal myogenesis in vivo and in vitro. Development 144, 2104–2122.

Chal, J., Oginuma, M., Al Tanoury, Z., Gobert, B., Sumara, O., Hick, A., Bousson, F., Zidouni, Y., Mursch, C., Moncuquet, P., et al. (2015). Differentiation of pluripotent stem cells to muscle fiber to model Duchenne muscular dystrophy. Nat. Biotechnol. 33, 962–969.

Chal, J., Al Tanoury, Z., Hestin, M., Gobert, B., Aivio, S., Hick, A., Cherrier, T., Nesmith, A.P., Parker, K.K., and Pourquié, O. (2016). Generation of human muscle fibers and satellite-like cells from human pluripotent stem cells in vitro. Nat. Protoc. 11, 1833–1850.

Chambers, S.M., Fasano, C.A., Papapetrou, E.P., Tomishima, M., Sadelain, M., and Studer, L. (2009). Highly efficient neural conversion of human ES and iPS cells by dual inhibition of SMAD signaling. Nat. Biotechnol. 27, 275–280.

Chavez, A., Scheiman, J., Vora, S., Pruitt, B.W., Tuttle, M., P R Iyer, E., Lin, S., Kiani, S., Guzman, C.D., Wiegand, D.J., et al. (2015). Highly efficient Cas9-mediated transcriptional programming. Nat. Methods 12, 326–328.

Chen, J.F., Tao, Y., Li, J., Deng, Z., Yan, Z., Xiao, X., and Wang, D.Z. (2010). microRNA-1 and microRNA-206 regulate skeletal muscle satellite cell proliferation and differentiation by repressing Pax7. J. Cell Biol. 190, 867–879.

Cheung, M., Tai, A., Lu, P.J., and Cheah, K.S. (2019). Acquisition of multipotent and migratory neural crest cells in vertebrate evolution. Curr. Opin. Genet. Dev. 57, 84–90.

De Micheli, A.J., Laurilliard, E.J., Heinke, C.L., Ravichandran, H., Fraczek, P., Soueid-Baumgarten, S., De Vlaminck, I., Elemento, O., and Cosgrove, B.D. (2020). Single-cell analysis of the muscle stem cell hierarchy identifies heterotypic communication signals involved in skeletal muscle regeneration. Cell Rep. 30, 3583–3595.e5.

Dell'Orso, S., Juan, A.H., Ko, K.D., Naz, F., Perovanovic, J., Gutierrez-Cruz, G., Feng, X., and Sartorelli, V. (2019). Single cell analysis of adult mouse skeletal muscle stem cells in homeostatic and regenerative conditions. Development 146, dev174177.

Flamini, V., Ghadiali, R.S., Antczak, P., Rothwell, A., Turnbull, J.E., and Pisconti, A. (2018). The satellite cell niche regulates the balance between myoblast differentiation and self-renewal via p53. Stem Cell Reports 10, 970–983.

Fu, Y., Sander, J.D., Reyon, D., Cascio, V.M., and Joung, J.K. (2014). Improving CRISPR-Cas nuclease specificity using truncated guide RNAs. Nat. Biotechnol. 32, 279–284.

Giordani, L., He, G.J., Negroni, E., Sakai, H., Law, J.Y.C., Siu, M.M., Wan, R., Corneau, A., Tajbakhsh, S., Cheung, T.H., and Le Grand, F. (2019). High-dimensional single-cell cartography reveals novel skeletal muscle-resident cell populations. Mol. Cell 74, 609–621.e6.

Gopinath, S.D., Webb, A.E., Brunet, A., and Rando, T.A. (2014). FOXO3 promotes quiescence in adult muscle stem cells during the process of self-renewal. Stem Cell Reports 2, 414–426.

Gros, J., and Tabin, C.J. (2014). Vertebrate limb bud formation is initiated by localized epithelial-to-mesenchymal transition. Science 343, 1253–1256.

Haghverdi, L., Buettner, F., and Theis, F.J. (2015). Diffusion maps for high-dimensional single-cell analysis of differentiation data. Bioinformatics 31, 2989–2998.

Hayashi, K., and Ozawa, E. (1995). Myogenic cell migration from somites is induced by tissue contact with medial region of the presumptive limb mesoderm in chick embryos. Development 121, 661–669.

Hicks, M.R., Hiserodt, J., Paras, K., Fujiwara, W., Eskin, A., Jan, M., Xi, H., Young, C.S., Evseenko, D., Nelson, S.F., et al. (2018). ERBB3 and NGFR mark a distinct skeletal muscle progenitor cell in human development and hPSCs. Nat. Cell Biol. 20, 46–57.

Joe, A.W., Yi, L., Natarajan, A., Le Grand, F., So, L., Wang, J., Rudnicki, M.A., and Rossi, F.M. (2010). Muscle injury activates resident fibro/adipogenic progenitors that facilitate myogenesis. Nat. Cell Biol. 12, 153–163.

Kim, J., Magli, A., Chan, S.S.K., Oliveira, V.K.P., Wu, J., Darabi, R., Kyba, M., and Perlingeiro, R.C.R. (2017). Expansion and purification are critical for the therapeutic application of pluripotent stem cell-derived myogenic progenitors. Stem Cell Reports 9, 12–22.

Kivelä, R., Salmela, I., Nguyen, Y.H., Petrova, T.V., Koistinen, H.A., Wiener, Z., and Alitalo, K. (2016). The transcription factor Prox1 is essential for satellite cell differentiation and muscle fibre-type regulation. Nat. Commun. 7, 13124.

Koopman, R., Ly, C.H., and Ryall, J.G. (2014). A metabolic link to skeletal muscle wasting and regeneration. Front. Physiol. 5, 32.

Langmead, B., and Salzberg, S.L. (2012). Fast gapped-read alignment with Bowtie 2. Nat. Methods 9, 357–359.

Li, X., Zhao, X., Fang, Y., Jiang, X., Duong, T., Fan, C., Huang, C.C., and Kain, S.R. (1998). Generation of destabilized green fluorescent protein as a transcription reporter. J. Biol. Chem. 273, 34970–34975.

Machado, L., Esteves de Lima, J., Fabre, O., Proux, C., Legendre, R., Szegedi, A., Varet, H., Ingerslev, L.R., Barrès, R., Relaix, F., and Mourikis, P. (2017). In situ fixation redefines quiescence and early activation of skeletal muscle stem cells. Cell Rep. 21, 1982–1993.

Macosko, E.Z., Basu, A., Satija, R., Nemesh, J., Shekhar, K., Goldman, M., Tirosh, I., Bialas, A.R., Kamitaki, N., Martersteck, E.M., et al. (2015). Highly parallel genome-wide expression profiling of individual cells using nanoliter droplets. Cell 161, 1202–1214.

Magli, A., and Perlingeiro, R.R.C. (2017). Myogenic progenitor specification from pluripotent stem cells. Semin. Cell Dev. Biol. 72, 87–98.

Mali, P., Yang, L., Esvelt, K.M., Aach, J., Guell, M., DiCarlo, J.E., Norville, J.E., and Church, G.M. (2013). RNA-guided human genome engineering via Cas9. Science 339, 823–826.

McConnell, B.B., and Yang, V.W. (2010). Mammalian Krüppel-like factors in health and diseases. Physiol. Rev. 90, 1337–1381.

Messina, G., Biressi, S., Monteverde, S., Magli, A., Cassano, M., Perani, L., Roncaglia, E., Tagliafico, E., Starnes, L., Campbell, C.E., et al. (2010). Nfix regulates fetal-specific transcription in developing skeletal muscle. Cell 140, 554–566.

Murmann, O.V., Niggli, F., and Schäfer, B.W. (2000). Cloning and characterization of the human PAX7 promoter. Biol. Chem. 381, 331–335.

Neufeld, S.J., Wang, F., and Cobb, J. (2014). Genetic interactions between Shox2 and Hox genes during the regional growth and development of the mouse limb. Genetics 198, 1117–1126.

Oginuma, M., Moncuquet, P., Xiong, F., Karoly, E., Chal, J., Guevorkian, K., and Pourquié, O. (2017). A gradient of glycolytic activity coordinates FGF and Wnt signaling during elongation of the body axis in amniote embryos. Dev. Cell 40, 342–353.e10.

Oh, Y., and Jang, J. (2019). Directed differentiation of pluripotent stem cells by transcription factors. Mol. Cells 42, 200–209.

Pala, F., Di Girolamo, D., Mella, S., Yennek, S., Chatre, L., Ricchetti, M., and Tajbakhsh, S. (2018). Distinct metabolic states govern skeletal muscle stem cell fates during prenatal and postnatal myogenesis. J. Cell Sci. 131, jcs212977.

Petchey, L.K., Risebro, C.A., Vieira, J.M., Roberts, T., Bryson, J.B., Greensmith, L., Lythgoe, M.F., and Riley, P.R. (2014). Loss of Prox1 in striated muscle causes slow to fast skeletal muscle fiber conversion and dilated cardiomyopathy. Proc. Natl. Acad. Sci. U S A *111*, 9515–9520.

Pistocchi, A., Gaudenzi, G., Foglia, E., Monteverde, S., Moreno-Fortuny, A., Pianca, A., Cossu, G., Cotelli, F., and Messina, G. (2013). Conserved and divergent functions of Nfix in skeletal muscle development during vertebrate evolution. Development *140*, 1528–1536.

Price, F.D., von Maltzahn, J., Bentzinger, C.F., Dumont, N.A., Yin, H., Chang, N.C., Wilson, D.H., Frenette, J., and Rudnicki, M.A. (2014). Inhibition of JAK-STAT signaling stimulates adult satellite cell function. Nat. Med. *20*, 1174–1181.

Quinlan, A.R., and Hall, I.M. (2010). BEDTools: a flexible suite of utilities for comparing genomic features. Bioinformatics *26*, 841–842.

Reinhardt, R., Gullotta, F., Nusspaumer, G., Ünal, E., Ivanek, R., Zuniga, A., and Zeller, R. (2019). Molecular signatures identify immature mesenchymal progenitors in early mouse limb buds that respond differentially to morphogen signaling. Development *146*, dev173328.

Rubenstein, A.B., Smith, G.R., Raue, U., Begue, G., Minchev, K., Ruf-Zamojski, F., Nair, V.D., Wang, X., Zhou, L., Zaslavsky, E., et al. (2020). Single-cell transcriptional profiles in human skeletal muscle. Sci. Rep. *10*, 229.

Ryall, J.G. (2013). Metabolic reprogramming as a novel regulator of skeletal muscle development and regeneration. FEBS J. *280*, 4004–4013.

Ryall, J.G., Dell'Orso, S., Derfoul, A., Juan, A., Zare, H., Feng, X., Clermont, D., Koulnis, M., Gutierrez-Cruz, G., Fulco, M., and Sartorelli, V. (2015). The NAD(+)-dependent SIRT1 deacetylase translates a metabolic switch into regulatory epigenetics in skeletal muscle stem cells. Cell Stem Cell *16*, 171–183.

Sacco, A., Doyonnas, R., Kraft, P., Vitorovic, S., and Blau, H.M. (2008). Self-renewal and expansion of single transplanted muscle stem cells. Nature *456*, 502–506.

Sambasivan, R., and Tajbakhsh, S. (2007). Skeletal muscle stem cell birth and properties. Semin. Cell Dev. Biol. *18*, 870–882.

Sanchez, A.M., Candau, R.B., and Bernardi, H. (2014). FoxO transcription factors: their roles in the maintenance of skeletal muscle homeostasis. Cell. Mol. Life Sci. *71*, 1657–1671.

Sartori, R., and Sandri, M. (2015). Bone and morphogenetic protein signalling and muscle mass. Curr. Opin. Clin. Nutr. Metab. Care *18*, 215–220.

Schiaffino, S., Rossi, A.C., Smerdu, V., Leinwand, L.A., and Reggiani, C. (2015). Developmental myosins: expression patterns and functional significance. Skelet. Muscle *5*, 22.

Schindelin, J., Arganda-Carreras, I., Frise, E., Kaynig, V., Longair, M., Pietzsch, T., Preibisch, S., Rueden, C., Saalfeld, S., Schmid, B., et al. (2012). Fiji: an open-source platform for biological-image analysis. Nat. Methods *9*, 676–682.

Schmidt, R., and Plath, K. (2012). The roles of the reprogramming factors Oct4, Sox2 and Klf4 in resetting the somatic cell epigenome during induced pluripotent stem cell generation. Genome Biol. *13*, 251.

Shea, K.L., Xiang, W., LaPorta, V.S., Licht, J.D., Keller, C., Basson, M.A., and Brack, A.S. (2010). Sprouty1 regulates reversible quiescence of a self-renewing adult muscle stem cell pool during regeneration. Cell Stem Cell *6*, 117–129.

Shelton, M., Metz, J., Liu, J., Carpenedo, R.L., Demers, S.P., Stanford, W.L., and Skerjanc, I.S. (2014). Derivation and expansion of PAX7-positive muscle progenitors from human and mouse embryonic stem cells. Stem Cell Reports *3*, 516–529.

Spandidos, A., Wang, X., Wang, H., and Seed, B. (2010). PrimerBank: a resource of human and mouse PCR primer pairs for gene expression detection and quantification. Nucleic Acids Res. *38*, D792–D799.

Subramanian, A., Tamayo, P., Mootha, V.K., Mukherjee, S., Ebert, B.L., Gillette, M.A., Paulovich, A., Pomeroy, S.L., Golub, T.R., Lander, E.S., and Mesirov, J.P. (2005). Gene set enrichment analysis: a knowledge-based approach for interpreting genome-wide expression profiles. Proc. Natl. Acad. Sci. U S A *102*, 15545–15550.

Tabula Muris Consortium; Overall Coordination; Logistical Coordination; Organ Collection and Processing; Library Preparation and Sequencing; Computational Data Analysis; Cell Type Annotation; Writing Group; Supplemental Text Writing Group; Principal Investigators (2018). Single-cell transcriptomics of 20 mouse organs creates a Tabula Muris. Nature *562*, 367–372.

Taglietti, V., Angelini, G., Mura, G., Bonfanti, C., Caruso, E., Monteverde, S., Le Carrou, G., Tajbakhsh, S., Relaix, F., and Messina, G. (2018). RhoA and ERK signalling regulate the expression of the transcription factor Nfix in myogenic cells. Development *145*, dev163956.

Takahashi, K., and Yamanaka, S. (2016). A decade of transcription factor-mediated reprogramming to pluripotency. Nat. Rev. Mol. Cell Biol. *17*, 183–193.

Tanaka, K., Matsumoto, E., Higashimaki, Y., Katagiri, T., Sugimoto, T., Seino, S., and Kaji, H. (2012). Role of osteoglycin in the linkage between muscle and bone. J. Biol. Chem. *287*, 11616–11628.

Tierney, M.T., and Sacco, A. (2016). Satellite cell heterogeneity in skeletal muscle homeostasis. Trends Cell Biol. *26*, 434–444.

Tierney, M.T., Aydogdu, T., Sala, D., Malecova, B., Gatto, S., Puri, P.L., Latella, L., and Sacco, A. (2014). STAT3 signaling controls satellite cell expansion and skeletal muscle repair. Nat. Med. *20*, 1182–1186.

Tierney, M.T., Gromova, A., Sesillo, F.B., Sala, D., Spenlé, C., Orend, G., and Sacco, A. (2016). Autonomous extracellular matrix remodeling controls a progressive adaptation in muscle stem cell regenerative capacity during development. Cell Rep. *14*, 1940–1952.

Tirosh, I., Izar, B., Prakadan, S.M., Wadsworth, M.H., 2nd, Treacy, D., Trombetta, J.J., Rotem, A., Rodman, C., Lian, C., Murphy, G., et al. (2016). Dissecting the multicellular ecosystem of metastatic melanoma by single-cell RNA-seq. Science *352*, 189–196.

Uezumi, A., Fukada, S., Yamamoto, N., Takeda, S., and Tsuchida, K. (2010). Mesenchymal progenitors distinct from satellite cells contribute to ectopic fat cell formation in skeletal muscle. Nat. Cell Biol. *12*, 143–152.

Uezumi, A., Nakatani, M., Ikemoto-Uezumi, M., Yamamoto, N., Morita, M., Yamaguchi, A., Yamada, H., Kasai, T., Masuda, S., Narita, A., et al. (2016). Cell-surface protein profiling identifies distinctive markers of progenitor cells in human skeletal muscle. Stem Cell Reports *7*, 263–278.

van den Brink, S.C., Sage, F., Vértesy, Á., Spanjaard, B., Peterson-Maduro, J., Baron, C.S., Robin, C., and van Oudenaarden, A. (2017). Single-cell sequencing reveals dissociation-induced gene expression in tissue subpopulations. Nat. Methods *14*, 935–936.

van Velthoven, C.T.J., de Morree, A., Egner, I.M., Brett, J.O., and Rando, T.A. (2017). Transcriptional profiling of quiescent muscle stem cells in vivo. Cell Rep. *21*, 1994–2004.

Xi, H., Fujiwara, W., Gonzalez, K., Jan, M., Liebscher, S., Van Handel, B., Schenke-Layland, K., and Pyle, A.D. (2017). In vivo human somitogenesis guides somite development from hPSCs. Cell Rep. *18*, 1573–1585.

Xu, C., Tabebordbar, M., Iovino, S., Ciarlo, C., Liu, J., Castiglioni, A., Price, E., Liu, M., Barton, E.R., Kahn, C.R., et al. (2013). A zebrafish embryo culture system defines factors that promote vertebrate myogenesis across species. Cell *155*, 909–921.

Xu, X., Wilschut, K.J., Kouklis, G., Tian, H., Hesse, R., Garland, C., Sbitany, H., Hansen, S., Seth, R., Knott, P.D., et al. (2015). Human satellite cell transplantation and regeneration from diverse skeletal muscles. Stem Cell Reports *5*, 419–434.

Yajima, H., Yoneitamura, S., Watanabe, N., Tamura, K., and Ide, H. (1999). Role of N-cadherin in the sorting-out of mesenchymal cells and in the positional identity along the proximodistal axis of the chick limb bud. Dev. Dyn. *216*, 274–284.

Yang, H., Wang, H., Shivalila, C.S., Cheng, A.W., Shi, L., and Jaenisch, R. (2013). One-step generation of mice carrying reporter and conditional alleles by CRISPR/Cas-mediated genome engineering. Cell *154*, 1370–1379.

Ye, J., Coulouris, G., Zaretskaya, I., Cutcutache, I., Rozen, S., and Madden, T.L. (2012). Primer-BLAST: a tool to design target-specific primers for polymerase chain reaction. BMC Bioinform. *13*, 134.

Yin, H., Price, F., and Rudnicki, M.A. (2013). Satellite cells and the muscle stem cell niche. Physiol. Rev. *93*, 23–67.

Yucel, N., Wang, Y.X., Mai, T., Porpiglia, E., Lund, P.J., Markov, G., Garcia, B.A., Bendall, S.C., Angelo, M., and Blau, H.M. (2019). Glucose metabolism drives histone acetylation landscape transitions that dictate muscle stem cell function. Cell Rep. *27*, 3939–3955.e6.

Zhao, P., and Hoffman, E.P. (2004). Embryonic myogenesis pathways in muscle regeneration. Dev. Dyn. *229*, 380–392.

Zhou, Y., Zhou, B., Pache, L., Chang, M., Khodabakhshi, A.H., Tanaseichuk, O., Benner, C., and Chanda, S.K. (2019). Metascape provides a biologist-oriented resource for the analysis of systems-level datasets. Nat. Commun. *10*, 1523.

STAR★METHODS

KEY RESOURCES TABLE

REAGENT or RESOURCE	SOURCE	IDENTIFIER
Antibodies		
Anti-PAX3	DSHB	Cat#: Pax3; RRID: AB_528426
Anti-PAX7	DSHB	Cat#: PAX7; RRID: AB_528428
Anti-MyHC	DSHB	Cat#: MF 20; RRID: AB_2147781
Anti-MET	Cell Signaling Technology	Cat# 8198; RRID: AB_10858224
Anti-CD325 (CDH2)	BD Biosciences	Cat#: 561553; RRID: AB_10713831
Anti-NANOG	Cell Signaling Technology	Cat# 3580; RRID: AB_2150399
Anti-OCT-4A	Cell Signaling Technology	Cat# 2840; RRID: AB_2167691
Anti-SOX2	Cell Signaling Technology	Cat# 3579; RRID: AB_2195767
Anti-PDGF Receptor alpha (PDGFRA)	Cell Signaling Technology	Cat# 3174; RRID: AB_2162345
Anti-M-Cadherin/Cadherin-15 (CDH15)	R&D Systems	Cat#: AF4096; RRID: AB_10641849
Anti-HGFR/c-MET (MET) - APC	R&D Systems	Cat#: FAB3582A; RRID: AB_1151927
Anti-CD325 (CDH2) - PE	BD Biosciences	Cat#: 561554; RRID: AB_10714646
Anti-CD31 – FITC	Thermo Fisher Scientific	Cat#: 11-0319-42; RRID: AB_2043835
Anti-CD31 – PE	Thermo Fisher Scientific	Cat#: 12-0319-42; RRID: AB_10669160
Anti-CD31 - APC/Cy7	BioLegend	Cat#: 303120; RRID: AB_10640734
Anti-CD45 - FITC	Thermo Fisher Scientific	Cat#: 11-0459-42; RRID: AB_10852703
Anti-CD45 – PE	Thermo Fisher Scientific	Cat#: 12-0459-42; RRID: AB_1724079
Anti-CD45 - APC/Cy7	BioLegend	Cat#: 368516; RRID: AB_2566376
Anti-CD235a - FITC	Thermo Fisher Scientific	Cat#: 11-9987-82; RRID: AB_465477
Anti-CD235a - PE	Thermo Fisher Scientific	Cat#: 12-9987-82; RRID: AB_466300
Anti- CD235a - APC/Cy7	BioLegend	Cat#: 349116; RRID: AB_ 2650978
Anti-ERBB3 - PE	BioLegend	Cat#: 324706; RRID: AB_2099569
Anti-CD271 (NGFR) - PerCP/Cy5.5	BioLegend	Cat#: 345111; RRID: AB_11204078
Anti-CD57 (HNK-1) - PE/Cy7	BioLegend	Cat#: 359624; RRID: AB_2632689
Anti-CD140a (PDGFRA) - PE	BD Biosciences	Cat#: 556002; RRID: AB_396286
Anti-CD140a (PDGFRA) - BV786	BD Biosciences	Cat#: 742669; RRID: AB_2740957
Anti-Rabbit IgG - Alexa Fluor Plus 488	Thermo Fisher Scientific	Cat#: A32731; RRID: AB_2633280
Anti-Mouse IgG2b - Alexa Fluor 568	Thermo Fisher Scientific	Cat#: A21144; RRID: AB_ 2535780
Anti-Sheep IgG - PerCP	Thermo Fisher Scientific	Cat#: A32731; RRID: AB_2633280
Anti-Mouse IgG1 - HRP	Thermo Fisher Scientific	Cat#: A10551; RRID: AB_2534048
Anti-Mouse IgG2a - HRP	Thermo Fisher Scientific	Cat#: A10685; RRID: AB_2534065
Anti-Mouse IgG2b - HRP	Thermo Fisher Scientific	Cat#: M32507; RRID: AB_2536649
Anti-Rabbit IgG - HRP	Promega	Cat#: W4011; RRID: AB_430833
Anti-Sheep IgG - PerCP	R&D Systems	Cat#: F0128; RRID: AB_10892337
Anti-Sheep IgG - NL557	R&D Systems	Cat#: NL010; RRID: AB_884220
Biological Samples		
Human embryos, fetuses and juvenile and adult skeletal muscle tissues	Table S1	N/A
Chemicals, Peptides, and Recombinant Proteins		
Y-27632	Tocris	Cat#: 1254; CAS#: 129830-38-2
CHIR99021	Tocris	Cat#: 4423; CAS#: 252917-06-9
LDN193189	Tocris	Cat#: 6053; CAS#: 1435934-00-1
SB431542	Tocris	Cat#: 1614; CAS#: 301836-41-9

(Continued on next page)

Continued

REAGENT or RESOURCE	SOURCE	IDENTIFIER
FGF2	Proteintech	Cat#: HZ-1285
HGF	PeproTech	Cat#: 100-39H
IGF1	Sigma-Aldrich	Cat#: I1271
mTeSR1	StemCell Technologies	Cat#: 85850
DMEM/F-12, HEPES medium	Thermo Fisher Scientific	Cat#: 11330032
DMEM, high glucose medium	Thermo Fisher Scientific	Cat#: 11965092
E6 medium	Thermo Fisher Scientific	Cat#: A4238501
StemPro-34 medium	Thermo Fisher Scientific	Cat#: 10639011
SkGM-2 Skeletal Muscle Cell Growth Medium-2 BulletKit	Lonza	Cat#: CC-3245
StemPro Osteogenesis Differentiation Kit	Thermo Fisher Scientific	Cat#: A1007201
ITS -G supplement	Thermo Fisher Scientific	Cat#: 41400045
N2 supplement	Thermo Fisher Scientific	Cat#: 17502048
Fetal bovine serum (FBS)	Thermo Fisher Scientific	Cat#: 16000044
Knockout Serum Replacement (KSR)	Thermo Fisher Scientific	Cat#: 10828028
GlutaMAX Supplement	Thermo Fisher Scientific	Cat#: 35050061
Nonessential amino acids (NEAA)	Thermo Fisher Scientific	Cat#: 11140076
Sodium Pyruvate	Thermo Fisher Scientific	Cat#: 11360070
2-Mercaptoethanol	Thermo Fisher Scientific	Cat#: 21985023; CAS#: 60-24-2
1-Thioglycerol	Sigma-Aldrich	Cat#: M6145; CAS#: 96-27-5
Matrigel hESC-Qualified	Corning	Cat#: 354277
TrypLE Express	Thermo Fisher Scientific	Cat#: 12605010
Collagenase, Type 2 (Collagenase II)	Worthington-Biochem	Cat#: LS004177
Collagenase IV	Thermo Fisher Scientific	Cat#: 17104019
Dispase II	Thermo Fisher Scientific	Cat#: 17105041
DNase I	Sigma-Aldrich	Cat#: D4513
Critical Commercial Assays		
PDMS chip - 26 Drop-seq generators on glass slide	FlowJEM	N/A
Barcoded beads for Drop-seq	ChemGenes	Cat#: MACOSKO-2011-1-0(V+)
Human TruStain FcX (Fc Receptor Blocking Solution)	BioLegend	Cat#: 422302
Alizarin S, 2% Solution, pH 4.2	Electron Microscopy Sciences	Cat#: 26206-01
TSA Plus Fluorescein	PerkinElmer	Cat#: NEL741001KT
TSA Plus TMR	PerkinElmer	Cat#: NEL742001KT
TSA Plus Cyanine 5	PerkinElmer	Cat#: NEL745001KT
RNAscope Multiplex Fluorescent Reagent Kit v2	Advanced Cell Diagnostics	Cat#: 323100
RNAscope 3-plex negative control probes	Advanced Cell Diagnostics	Cat#: 320871
RNAscope Probe - Hs-NFIX	Advanced Cell Diagnostics	Cat#: 522341
RNAscope Probe - Hs-KLF9-C2	Advanced Cell Diagnostics	Cat#: 582551-C2
RNAscope Probe - Hs-NFIC	Advanced Cell Diagnostics	Cat#: N/A; custom ordered new probe
RNAscope Probe - Hs-CEBPD	Advanced Cell Diagnostics	Cat#: N/A; custom ordered new probe
RNeasy Plus Mini Kit	QIAGEN	Cat#: 74134
RNeasy Plus Micro Kit	QIAGEN	Cat#: 74034
iScript Reverse Transcription Supermix for RT-qPCR	Bio-Rad	Cat#: 1708841
SsoAdvanced Universal SYBR Green Supermix	Bio-Rad	Cat#: 1725274
Gibson Assembly Cloning Kit	New England BioLabs	Cat#: E5510S
NEBuilder HiFi DNA Assembly Master Mix	New England BioLabs	Cat#: E2621S
P3 Primary Cell 4D-Nucleofector X Kit L	Lonza	Cat#: V4XP-3024
ViaFect Transfection Reagent	Promega	Cat#: E4981

Continued

REAGENT or RESOURCE	SOURCE	IDENTIFIER
Deposited Data		
Raw sequencing reads and processed DGE matrices	This paper	GEO: GSE147457
Interactive scRNA-seq exploration tools	This paper	skeletal-muscle.cells.ucsc.edu or aprilpylelab.com/datasets
Experimental Models: Cell Lines		
Human: H9 (WA09) hESC line	WiCell	RRID: CVCL_9773
Human: PAX7-GFP reporter lines derived from H9 cells	This Paper	N/A
Oligonucleotides		
Forward sequence for cloning gRNA for homologous recombination of reporter cassette to the *PAX7* locus: GTGAGTG GGTGTACGTGGTTTTAGAGCTAGAAA TAGCAAGTTAAAATAAGGCTAGTC	This paper	N/A
Reverse sequence for cloning gRNA for homologous recombination of reporter cassette to the *PAX7* locus: CACGTAC ACCCACTCACGGTGTTTCGTCCTTTC CACAAGATATATAAAGCCAAGAAA	This paper	N/A
Forward sequence for cloning gRNA targeting *PAX7* promoter region for gene activation (Pax7C3): GTCAAAC GCGTCCAGAAGCTGTTTTAGAGCTAG AAATAGCAAGTTAAAATAAGGCTAGTC	This paper	N/A
Reverse sequence for cloning gRNA targeting *PAX7* promoter region for gene activation (Pax7C3): AGCTTCTGGACGCGTTTGACGGTG TTTCGTCCTTTCCACAAGATATATAAAGCCAAGAAA	This paper	N/A
Forward sequence for cloning gRNA targeting *PAX7* promoter region for gene activation (Pax7C4): GGGGCCAAAGTTTCCGAGCCGTTTTAGAGC TAGAAATAGCAAGTTAAAATAAGGCTAGTC	This paper	N/A
Reverse sequence for cloning gRNA targeting *PAX7* promoter region for gene activation (Pax7C4): GGCTCGGAAACTTTGGCCCCGGTGTTTCGT CCTTTCCACAAGATATATAAAGCCAAGAAA	This paper	N/A
Forward sequence for cloning gRNA targeting *PAX7* promoter region for gene activation (Pax7C5): GGGTCCGGAGAAAGAAGGCGGTTTTAGAG CTAGAAATAGCAAGTTAAAATAAGGCTAGTC	This paper	N/A
Reverse sequence for cloning gRNA targeting *PAX7* promoter region for gene activation (Pax7C5): CGCCTTCTTTCTCCGGACCCGGTGTTTCGT CCTTTCCACAAGATATATAAAGCCAAGAAA	This paper	N/A
Forward sequence for cloning gRNA targeting *PAX7* promoter region for gene activation (Pax7C6): GCCCCGGCTCGACCTCGTTTGTTTTAGAGC TAGAAATAGCAAGTTAAAATAAGGCTAGTC	This paper	N/A
Reverse sequence for cloning gRNA targeting *PAX7* promoter region for gene activation (Pax7C6): AAACGAGGTCGAGCCGGGGCGGTGTTTCG TCCTTTCCACAAGATATATAAAGCCAAGAAA	This paper	N/A
Primer pairs for qRT-PCR	Xi et al., 2017 Methods S1	N/A

(Continued on next page)

Continued

REAGENT or RESOURCE	SOURCE	IDENTIFIER
Recombinant DNA		
gRNA_Cloning Vector	Mali et al., 2013	RRID: Addgene_41824
hCas9	Mali et al., 2013	RRID: Addgene_41815
Oct4-IRES-eGFP-PGK-Neo	Yang et al., 2013	RRID: Addgene_48681
SP-dCas9-VPR	Chavez et al., 2015	RRID: Addgene_63798
Software and Algorithms		
Drop-seq_tools-1.13	Macosko et al., 2015	https://github.com/broadinstitute/Drop-seq/releases/tag/v1.13
Bowtie2 v2.2.9	Langmead and Salzberg, 2012	http://bowtie-bio.sourceforge.net/bowtie2/index.shtml
Bedtools v2.26.0	Quinlan and Hall, 2010	https://github.com/arq5x/bedtools2
Seurat v2.3.3	Butler et al., 2018	https://github.com/satijalab/seurat/releases/tag/v2.3.3
Monocle3	Cao et al., 2019	https://cole-trapnell-lab.github.io/monocle3/
Pheatmap v1.0.12	The Comprehensive R Archive Network	https://cran.r-project.org/web/packages/pheatmap/index.html
Eulerr v6.0.0	The Comprehensive R Archive Network	https://cran.r-project.org/web/packages/eulerr/index.html
Metascape	Zhou et al., 2019	http://metascape.org/gp/index.html#/main/step1
GSEA	Subramanian et al., 2005	https://www.gsea-msigdb.org/gsea/index.jsp
Gene network analysis	This paper	In STAR Methods; Will be provided upon request
Fiji/ImageJ	Schindelin et al., 2012	http://fiji.sc/
ZEN 3.1 (blue edition) and ZEN 2.6 Pro (blue edition)	ZEISS	https://www.zeiss.com/microscopy/int/products/microscope-software/zen.html
PrimerBank	Spandidos et al., 2010	https://pga.mgh.harvard.edu/primerbank/
Primer-BLAST	Ye et al., 2012	https://www.ncbi.nlm.nih.gov/tools/primer-blast/
FlowJo	FlowJo, LLC	https://www.flowjo.com/

RESOURCE AVAILABILITY

Lead Contact
Further information and requests for resources and reagents should be directed to and will be fulfilled by the Lead Contact, April D. Pyle (apyle@mednet.ucla.edu).

Materials availability
Plasmids generated in this study will be provided upon request.

Data and code availability
Both raw sequencing reads and processed digital gene expression (DGE) matrices of scRNA-seq datasets are deposited at NCBI GEO with accession number GEO: GSE147457. Interactive scRNA-seq data exploration can be accessed at skeletal-muscle.cells.ucsc.edu or aprilpylelab.com/datasets. General codes for computational analysis follow the instructions of the respective software and customized modifications will be available upon request.

EXPERIMENTAL MODEL AND SUBJECT DETAILS

Human tissues
Human tissues of 9 weeks of gestation or younger were obtained from electively aborted embryos and fetuses following informed consent and de-identification in accordance with institutional guidelines, which was approved by the local research ethics committee of the University of Tübingen (#312/2016BO1 and #634/2017BO1). Human tissues of 12-18 weeks of gestation were obtained from

the University of California Los Angeles (UCLA) Center for AIDS Research (CFAR) Gene and Cellular Therapy Core using institutional review board (IRB)-approved de-identified and consented electively aborted human fetuses. Skeletal muscles from the 7 years old human juvenile subject were obtained from leftover tissues from surgical procedures approved by the UCLA institutional IRB, with patient consent and de-identification. Skeletal muscles from the 11 years old human juvenile subject and the two adult human subjects were obtained from donor autopsy provided by the National Disease Research Interchange (NDRI) with de-identification. Use of human tissues was IRB exempt by the UCLA Office of the Human Research Protection Program (IRB #15-000959).

Cell lines
The H9 human embryonic stem cells (WA09; WiCell Research Institute) are registered in the NIH Human Embryonic Stem Cell Registry with the Approval Number: NIH hESC-10-0062 (https://grants.nih.gov/stem_cells/registry/current.htm?id=414). The PAX7-GFP reporter cell lines are derived from the H9 cells.

METHOD DETAILS

Cell preparation for single cell RNA-sequencing
Embryonic week 7.25 and younger samples
Whole limbs were washed with wash buffer consisting of DMEM/F12, 10% fetal bovine serum (FBS), 1% Penicillin-Streptomycin (P/S) and 0.1% Amphotericin. Tissues were then mechanically chopped into small pieces at room temperature (RT) in digestion buffer consisting of wash buffer supplemented with 2 mg/ml of Collagenase IV and 1 mg/ml of Dispase II. Chopped tissues were further incubated in digestion buffer on a shaker at 37°C for 10-20 minutes with intermittent trituration. Digestion was stopped by adding surplus amount of Drop-seq buffer consisting of phosphate-buffered saline (PBS) supplemented with 0.01% bovine serum albumin (BSA). Digested tissues were filtered twice through 40 μm cell strainers, spun down and resuspended in small volumes of Drop-seq buffer. Cell number was counted and resuspended cells were kept on ice until subjected to the Drop-seq flow procedures.

Embryonic week 7.75 and fetal week 9 samples
Whole limbs excluding feet were washed with wash buffer and then mechanically chopped into small pieces at RT in digestion buffer consisting of wash buffer supplemented with 2 mg/ml of Collagenase II and 1 mg/ml of Dispase II. Chopped tissues were further incubated in digestion buffer on a shaker at 37°C for 20-25 minutes with intermittent trituration. Digestion was stopped by adding surplus amount of Drop-seq buffer. Digested tissues were filtered twice through 40 μm cell strainers, spun down and resuspended in small volumes of Drop-seq buffer. Cell number was counted and resuspended cells were kept on ice until subjected to the Drop-seq flow procedures.

Fetal week 12-18 samples
Skeletal muscles from whole limbs were separated from bones and skin. Muscles were washed with wash buffer and then mechanically chopped into small pieces at RT in digestion buffer consisting of wash buffer supplemented with 2 mg/ml of Collagenase II, 1 mg/ml of Dispase II and 50 μg/ml of DNase I. Chopped tissues were further incubated in digestion buffer on a shaker at 37°C for 20-25 minutes with intermittent trituration. Digestion was stopped by adding surplus amount of fluorescence-activated cell sorting (FACS) buffer consisting of PBS supplemented with 1% FBS and 1% P/S. Digested tissues were filtered through 100 μm cell strainers and spun down. Cell pellets were resuspended in FACS buffer, filtered through 70 μm cell strainers, spun down and resuspended again in small volumes of FACS buffer. Cells were then incubated on ice with antibodies against CD31, CD45 and CD235a. Stained cells were sorted on BD FACSAria sorters to collect the DAPI⁻/CD31⁻/CD45⁻/CD235a⁻ fraction (live and depletion of the endothelial and hematopoietic lineages). Sorted cells were washed with Drop-seq buffer, spun down and resuspended in small volumes of Drop-seq buffer. Cell number was counted and resuspended cells were kept on ice until subjected to the Drop-seq flow procedures.

Postnatal juvenile and adult samples
Skeletal muscles from autopsy or surgical procedures were washed with wash buffer and then mechanically chopped into small pieces at RT in primary digestion buffer consisting of wash buffer supplemented with 2 mg/ml of Collagenase II. Chopped tissues were further incubated in primary digestion buffer on a shaker at 37°C for 10-20 minutes with intermittent trituration. Primary digestion was stopped by adding surplus amount of wash buffer and tissues spun down. Next, supernatant was removed and tissues were resuspended in secondary digestion buffer consisting of wash buffer supplemented with 7 mg/ml of Collagenase D, 1.5 mg/ml of Dispase II and 50 μg/ml of DNase I. Tissues were further digested on a shaker at 37°C for 15-20 minutes with intermittent trituration. Secondary digestion was stopped by adding surplus amount of FACS buffer. Digested tissues were filtered through 100 μm cell strainers and spun down. Cell pellets were resuspended in FACS buffer, filtered through 70 μm cell strainers, spun down and resuspended again in small volumes of FACS buffer. Cells were then incubated on ice with antibodies against CD31, CD45 and CD235a. Stained cells were sorted on BD FACSAria sorters to collect the DAPI⁻/CD31⁻/CD45⁻/CD235a⁻ fraction (live and depletion of the endothelial and hematopoietic lineages). Sorted cells were washed with Drop-seq buffer, spun down and resuspended in small volumes of Drop-seq buffer. Cell number was counted and resuspended cells were kept on ice until subjected to the Drop-seq flow procedures.

Human pluripotent stem cell-derived samples
At the end of directed differentiation, cells were dissociated by 2 mg/ml of Collagenase IV for about 5 min, followed by TrypLE Express for another 5-7 minutes. Dissociation was stopped by adding surplus amount of FACS buffer and dissociated cells were filtered sequentially through 100 and 70 μm cell strainers. Cells were spun down and resuspended in small volumes of FACS buffer. For

some samples, cells were incubated on ice with antibodies against ERBB3, NGFR and HNK1. Cells were sorted on BD FACSAria sorters to collect the total live (DAPI⁻), DAPI⁻/ERBB3⁺/NGFR⁺/HNK1⁻ or DAPI⁻/GFP⁺ fractions. Sorted cells were washed with Drop-seq buffer, spun down and resuspended in small volumes of Drop-seq buffer. Cell number was counted and resuspended cells were kept on ice until subjected to the Drop-seq flow procedures.

Cell capture and library construction for single cell RNA-sequencing
Prepared single cell solutions were subjected to single cell capture and droplet formation following instructions in the online Drop-seq protocol v.3.1 (http://mccarrolllab.org/download/905/) and those published in the original Drop-seq paper (Macosko et al., 2015). In brief, cells at 150,000 cells/ml, barcoded beads at 175,000 beads/ml and droplet generation oil were co-flowed at a rate of 4, 4, and 15 ml/hour, respectively, in a PDMS microfluidics chip to generate oil droplets containing beads and lysed cells. Post flow, droplets were breakdown and reverse transcription performed. Complementary DNA was PCR amplified, magnetically cleaned up and subjected to tagmentation and sequencing library construction. Prepared libraries were cleaned up and sequenced via Illumina Hi-Seq2500, HiSeq4000 or NovaSeq.

Human PSC maintenance
The parental H9 cells and engineered PAX7-GFP reporter cells were maintained on Matrigel-coated tissue culture plates in mTeSR1 medium. Cells were fed with fresh medium every day and passaged with 0.5 mM of EDTA every 4-6 days.

Human PSC skeletal myogenic directed differentiation
HX protocol
Differentiation was performed following procedures published by Xi et al. (Xi et al., 2017) with minor modifications. Briefly, on day −1 hPSC colonies were dissociated into single cells with TrypLE Express and seeded on Matrigel-coated tissue culture plates at 12,500-25,000 cells/cm² in mTeSR1 medium containing 10 μM of Y-27632. Differentiation was initiated the next day (day 0) when medium was switched to DMEM/F12 medium containing 1% ITS-G, 0.5% P/S and 3 μM of CHIR99021 (CHIR) for 2 days. On day 2, cells were switched to DMEM/F12 medium containing 1% ITS-G, 0.5% P/S, 200 nM of LDN193189 (LDN) and 10 μM of SB431542 (SB) for another 2 days. On day 4, LDN and SB from the previous medium were replaced with 10 μM of CHIR and 20 ng/ml of FGF2 for 2 days. On day 6, medium was switched to DMEM medium containing 0.5% P/S, 15% KSR (Knockout Serum Replacement), 10 ng/ml of HGF and 2 ng/ml of IGF1 until the end of differentiation. Cells were fed with fresh medium every day until day 6 and every other day thereafter.

JC protocol
Differentiation was performed following procedures published by Chal et al. (Chal et al., 2015; Chal et al., 2016). Briefly, on day −1 hPSC colonies were dissociated into single cells with TrypLE Express and seeded on Matrigel-coated tissue culture plates at 15,000 cells/cm² in mTeSR1 medium containing 10 μM of Y-27632. Differentiation was initiated on day 0 by switching to a medium containing DMEM/F12, 1% ITS-G, 1% nonessential amino acids (NEAA) and 0.5% P/S supplemented with 3 μM of CHIR and 0.5 μM of LDN. On day 3, 20 ng/ml of FGF2 was added to the differentiation medium for an additional 3 days. On day 6, medium was changed to a medium containing DMEM/F12, 15% KSR, 1% NEAA, 0.5% P/S and 0.1 mM of 2-mercaptoethanol supplemented with 10 ng/ml of HGF, 2 ng/ml of IGF1, 20 ng/ml of FGF2 and 0.5 μM of LDN for 2 days. On day 8, medium was changed to DMEM/F12 containing 15% KSR, 1% NEAA, 0.5% P/S and 0.1 mM of 2-mercaptoethanol supplemented with 2 ng/ml of IGF1. On day 12 until the end of differentiation, 10 ng/ml of HGF was added to the previous medium. Cells were fed with fresh medium every day until day 12 and every other day thereafter.

MS protocol
Differentiation was performed following procedures published by Shelton et al. (Shelton et al., 2014) with minor modifications (Hicks et al., 2018). Briefly, on day −1 hPSC colonies were dissociated into single cells with TrypLE Express and seeded on Matrigel-coated tissue culture plates at 37,500 cells/cm² in mTeSR1 medium containing 10 μM of Y-27632. On the next day (day 0), differentiation was initiated by switching to the E6 medium containing 0.5% P/S supplemented with 10 μM of CHIR for 2 days. On day 2, cells were switched to E6 medium containing 0.5% P/S for 10 days. On day 12, medium was changed to StemPro-34 medium supplemented with 0.5% P/S, 2 mM of L-glutamine, 0.45 mM of 1-thioglycerol, 11 μg/ml of human transferrin and 5 ng/ml of FGF2 for 6 to 8 days. On around day 20, medium was switched to E6 medium containing 0.5% P/S for about 10-15 days with the medium during the last 5-7 days of this period supplemented with 10 ng/ml of IGF1. From around day 30-35, medium was changed to DMEM/F12 containing 1.2% N2 supplement, 1% ITS-G, 0.5% P/S and 10 ng/ml of IGF1 for about 5 days. From then on cells were cultured in the same medium supplemented with 3 μM of SB until the end of differentiation. Cells were fed with fresh medium every day.

PAX7-GFP reporter cell construction
Candidate guide RNAs (gRNAs) targeting the 3′ untranslated region (UTR) of *PAX7* transcript variant 3, which is conserved across species, were designed using the online tool at http://zlab.bio/guide-design-resources. The targeting region was limited to the last 1600 bp of the 3′ UTR to exclude the potential human miR206/miR1-1/miR1-2 binding sites predicted by miRBase (http://www.mirbase.org/), as the mouse counterparts of these miRNAs have been shown to regulate *Pax7* expression (Chen et al., 2010). Next, each of the candidate gRNAs in both the regular 20 bp form and short 17 bp form (which has been reported to increase specificity by Fu et al. [2014]) was cloned into a gRNA cloning vector (Addgene, #41824; [Mali et al., 2013]) using the Gibson Assembly

Cloning Kit following manufacturer's instructions. The final gRNA used was selected based on the highest cleavage efficiencies in hPSCs when a hCas9 plasmid (Addgene, #41815; [Mali et al., 2013]) was co-expressed. The *PAX7* targeting homology arms were then PCR amplified from the H9 cell genomic DNA based on the gRNA targeting region selected. For homologous recombination (HR) vector, the Oct4-IRES-eGFP-PGK-Neo plasmid (Addgene, #48681; [Yang et al., 2013]) was used and the *Oct4* targeting homology arms were replaced by the ones targeting *PAX7* using the Gibson Assembly Cloning Kit following manufacturer's instructions. Plasmids encoding gRNA, hCas9 and the HR construct (2 μg each) were nucleofected together into 800,000 H9 cells following the Lonza Amaxa 4D guideline with program CA-137. Four days post nucleofection, neomycin/G418 selection at 50 μg/ml was applied for 5 days and then increased to 100 μg/ml afterward. Individual resistant clones were expanded and genotyped to confirm correct insertion of the reporter cassette. One of the confirmed clones was incubated with recombinant TAT-Cre protein (a gift from Dr. William Pastor, McGill University) to remove the PGK-neomycin cassette between the LoxP sites. Single cell clones were selected, expanded and confirmed by genotyping and they regained sensitivity to neomycin/G418. Two of the final clones, #13 and #22 were used for downstream functional validation and clone #22 were used for directed differentiation for scRNA-seq experiments. Both clones were confirmed to express the pluripotency markers (NANOG, OCT4 and SOX2) by immunofluorescence staining. They were also examined and showed normal karyotypes.

PAX7-GFP reporter validation
Method of dCas9-VPR
Four gRNAs targeted to the *PAX7* promoter region (Murmann et al., 2000) were designed using http://zlab.bio/guide-design-resources. Each gRNA was cloned individually into the gRNA cloning vector (Addgene, #41824) similarly to previously described (Mali et al., 2013). In brief, 50 ng AflII-digested empty gRNA plasmid was mixed with 3.8 ng of the forward and reverse oligos and combined using the NEBuilder HiFi DNA Assembly Master Mix according to the manufacturer's instructions. To activate endogenous *PAX7* locus, plasmids encoding for all 4 gRNAs along with one for dCas9-VPR (Addgene, #63798; [Chavez et al., 2015]) were co-transfected using ViaFect according to manufacturer's instructions. To limit nucleofection-related toxicity and increase transfection efficiency, H9 cells were dissociated into single cells with TrypLE Express and seeded on Matrigel-coated tissue culture plates at 25,000 cells/cm^2 in mTeSR1 medium containing 10 μM of Y-27632. The next day medium was changed to DMEM/F12 medium containing 1% ITS-G, 0.5% P/S and 3 μM of CHIR for 2 days. One day before transfection, cells were dissociated into single cells and seeded on Matrigel-coated tissue culture plates at 75,000 cells/cm^2 in DMEM medium supplemented with 20% FBS, 1% chicken embryo extract and 20 ng/ml of FGF2. One day after, cells were co-transfected in the same medium with 0.5 μg of each plasmids. Cells were grown for 3 more days with medium changing every day to express the vectors and activate the PAX7-GFP reporter cassette. Cells were then harvested and purified by FACS. Cells co-transfected with dCas9-VPR plasmid and the empty gRNA vector were used as controls. The GFP$^+$ and GFP$^-$ cell fractions were collected and subjected to downstream analysis.
Method of directed differentiation
PAX7-GFP reporter cells were subjected to directed differentiation by the HX protocol as described above. Cells were harvested and purified by FACS. The H9 parental cells were differentiated alongside the reporter cells and used as controls. The GFP$^+$ and GFP$^-$ cell fractions were collected and subjected to downstream analysis.

FACS cell sorting
Single cell solutions were filtered through 40 μm cell strainers and incubated with 1 μg/ml of DAPI as a live/dead cell indicator. When cell surface labeling was needed, cells were first blocked by Human TruStain FcX at RT for 5-10 minutes, followed by fluorophore-conjugated primary antibodies on ice for 20-30 minutes. For antigens requiring 2-step antibody staining, cells were stained on ice for 20-30 minutes with unconjugated primary antibodies followed by fluorophore-conjugated secondary antibodies on ice for another 20-30 minutes. Stained cells were washed with FACS buffer and processed as described above. Cells were sorted by BD FACSAria sorters with FACSDiva software. Standard gating strategies were applied to exclude the debris, doublets and dead cells. Marker specific gating was set up using fluorescence-minus-one stained controls. The parental H9 cells were used for GFP gating. Sorted cells were collected into buffers containing 10% FBS and kept cold until downstream processing. FACS plots were generated using FlowJo.

Immunofluorescence
Cells were fixed with 4% PFA for 10 minutes, followed by permeabilization with 0.3% Triton X-100 in PBS at RT for 10 minutes at RT. Samples were then blocked with 3% BSA, 10% goat serum and 0.3% Triton X-100 in PBS for 60 minutes at RT. Primary antibodies were applied for overnight at 4°C and fluorophore-conjugated secondary antibodies for 60 minutes at RT. Nuclei were counter stained with DAPI at 1 μg/ml. Images were captured using a Zeiss Axio Observer.Z1 microscope equipped with an AxioCamMR3 camera. Image processing and quantification were performed using Fiji/ImageJ (Schindelin et al., 2012) or Zeiss ZEN 3.1 (blue edition).

Cytospin
Sorted cells were spun down onto Superfrost Plus microscope slides using Shandon Double Cytofunnel in a Shandon Cytocentrifuge. Attached cells were processed for immunofluorescence (IF) staining and imaging as described above.

Immunohistochemistry with tyramide signal amplification

Human embryos and tissues were fixed with 4% PFA for one day at 4°C, washed and embedded in paraffin. To reduce tissue auto-fluorescence for samples of fetal week 9 and older, they were subjected to a dehydration-bleaching-rehydration process before embedding as described by The Collection of Immunolabeled Transparent Human Embryos and Fetuses project (https://transparent-human-embryo.com/?page_id=649) (Belle et al., 2014). Tissue blocks were then sectioned at a 4 μm interval onto Super-frost Plus microscope slides. For immunohistochemistry (IHC) staining, sections were deparaffinized with Xylene and rehydrated through EtOH/water gradient. Antigen retrieval was performed with a pressure cooker using 10 mM of sodium citrate buffer, followed by blocking with 3% BSA, 10% goat serum and 0.1% Tween-20 in PBS for 60 minutes at RT. Primary antibodies were applied for overnight at 4°C and HRP-conjugated secondary antibodies were applied for 45-60 minutes at RT. Tyramide signal amplification (TSA) was performed using the TSA Plus Fluorescence kits per the manufacturer's instructions to amplify the fluorescent signals. Slides were mounted with DAPI nuclei counterstaining and proceeded to image capture and analysis as described above. Images showing whole limbs of early embryonic development were captured in a mosaic mode and stitched together using the Zeiss software.

RNAscope with Immunohistochemistry

Human tissues were processed similar to regular IHC procedures as described above, except that fixation was performed at RT instead of 4°C and the bleaching step was omitted according to manufacturer's recommendations. Sections were hybridized with cataloged or custom-designed RNAscope probes and signal developed per manufacturer's instructions using the RNAscope Multi-plex Fluorescent Reagent Kit v2, with in-house protease treatment optimization (Protease Plus 15 minutes). Probe-hybridized sections were further subjected to IHC staining of PAX7 with TSA and imaged as described above. Quantification of RNAscope signals and PAX7 cells was performed using Zeiss ZEN 2.6 Pro (blue edition) software. RNAscope negative probes were applied on sections from different individual samples to set the threshold for positive signal counting.

Quantitative real time-PCR

Cells were harvested and RNA extracted using RNeasy Plus Mini or Micro Kit. Complementary DNA was synthesized using iScript Reverse Transcription Supermix and quantitative real time-PCR (qRT-PCR) was performed using SsoAdvanced Universal SYBR Green Supermix with technical triplicates on a Bio-Rad CFX384 Touch Real-Time PCR Detection System or a Thermo Fisher Scientific QuantStudio 6 Pro Real-Time PCR System. All primer pairs were selected from PrimerBank (Spandidos et al., 2010) or designed using Primer-BLAST (Ye et al., 2012) and tested in-house to ensure an amplification efficiency between 90%–110%. Primer sequences for *BGLAP*, *CKM*, *DCN*, *eGFP*, *IBSP*, *MYH8*, *OGN* and *RPL13A* are listed in Methods S1. Other primer pairs are the same as previously reported (Xi et al., 2017).

In vitro myotube fusion assay

Sorted cells were resuspended in Lonza SkGM2 medium supplemented with 20 ng/ml of FGF2 and plated onto Matrigel-coated culture wells. Cells were cultured for 5-7 days until they reached > 70%–80% confluency. Then, medium was switched to DMEM/F12 medium containing 1% ITS-G, 0.5% P/S and 1% N2 supplement to induce fusion for 4-6 days. Medium was refreshed every other day during the culture, and cells at the end of fusion were subjected to IF staining and imaging as described above.

In vitro myogenic and osteogenic bipotential differentiation assays

Sorted cells were plated onto Matrigel-coated culture wells and expanded for 4-6 days in expansion medium (DMEM/F12 medium containing 20% FBS, 1% GlutaMAX, 1% NEAA, 1mM sodium pyruvate, 0.5% P/S and 20 ng/ml of FGF2). Cells were then split and cultured for another 2-3 days in expansion medium until they reached > 70%–80% confluency. For myogenic differentiation, medium was switched to fusion medium for 4-6 days as described above and cells were subjected to IF staining or harvested for qRT-PCR at the end of the fusion period. For osteogenic differentiation, medium was switched to Thermo Fisher Scientific StemPro Osteogenesis Differentiation medium for 2-3 weeks. At the end of the osteogenic period, cells were subjected to Alizarin Red S staining as previously reported (Xi et al., 2017) or harvested for qRT-PCR analysis. Medium was refreshed every other day during expansion and differentiation.

QUANTIFICATION AND STATISTICAL ANALYSIS

Processing, read alignment and digital gene expression matrix generation

The raw sequencing reads were processed using the Drop-seq_tools-1.13 pipeline from the McCaroll lab (https://github.com/broadinstitute/Drop-seq/releases/tag/v1.13), following the general guidelines from the Drop-seq Alignment Cookbook v1.2 (https://github.com/broadinstitute/Drop-seq/files/2425535/Drop-seqAlignmentCookbookv1.2Jan2016.pdf) (Macosko et al., 2015). Briefly, reads were indexed and filtered by read quality. Sequencing adaptor and polyA sequences were trimmed, and reads were further filtered to retain those of a length of at least 30 nucleotides. Processed reads were aligned to the human reference genome (hg19) using Bowtie2 (v2.2.9 with the '–very-sensitive' mode) (http://bowtie-bio.sourceforge.net/bowtie2/index.shtml) (Langmead and Salzberg, 2012). Aligned reads were tagged to gene exons using Bedtools Intersect (v2.26.0) (https://github.com/arq5x/bedtools2) (Quinlan and Hall, 2010). Knee plots of cell-to-read fraction were generated to estimate the number of cell barcodes

representing true cells. Digital gene expression matrices (DGEs) were then generated by counting gene transcripts for the number of cell barcodes selected based on the infliction points in the knee plots. To correct for any bead synthesis errors/read errors leading to false barcodes, transcript barcodes (unique molecular identifiers; UMIs) or cell barcodes were merged when they were within 1 Hamming or 2 Levenshtein distances, respectively. Barcodes containing < 2500 reads were excluded from the DGEs.

Computational analysis using Seurat
Data filtration, normalization and scaling
Downstream computational analyses of scRNA-seq data were mainly performed using the R package Seurat v2.3.3 (https://github.com/satijalab/seurat/releases/tag/v2.3.3) (Butler et al., 2018) by largely following the standard guidelines from the Satija lab (https://satijalab.org/seurat/). Seurat objects were generated with DGEs constructed as described above. Violin plots of number of expressed genes and unique transcripts (nGene and nUMI, respectively) of each cell were generated and outliers with too high or too low nGene and nUMI were removed to exclude potential cell doublets/aggregates or low quality cells/cell debris, respectively. As sequencing depth and cell type compositions vary across different samples, this filtration step was performed on a sample-to-sample basis. In general, prenatal and hPSC-derived samples were filtered with a minimum nGene of 500-1000. We consistently observed lower number of genes expressed from postnatal juvenile and adult samples, although in general they have the lowest unique read fraction levels (suggesting higher sequencing coverage) among all samples. Therefore, we set the nGene threshold of these samples to 250-400. After the cell filtration step, expression counts of each cell were normalized with the default Seurat setting using "NormalizeData." To mitigate the cell cycle effects on potentially grouping different cell types based on their cell cycle states, we assigned "S.Score" and "G2M.Score" on each cell with the average normalized expression levels of core cell cycle genes using "CellCycleScoring" following the Seurat instructions (Tirosh et al., 2016). To reduce the effects of dissociation-related stress on gene expression analysis, we obtained the core stress genes identified from scRNA-seq studies on both mouse skeletal muscle and acinar (van den Brink et al., 2017) (Table S7), and assigned each cell a "Stress" score using the core stress gene list through the Seurat "AddModuleScore" function. Briefly, this function first assigned each of the genes to be analyzed into different bins based on the genes' average expression across single cells. It then calculated a residual for each analyzed gene in each cell by subtracting the average expression of the control gene set from the expression level of the gene being analyzed, where the control genes were randomly selected from the bin that the analyzed gene was assigned to. This process was then reiterated through all the genes in the provided list, and the resulted aggregated expression was assigned as the score of the property the provided gene list represents. After this step, data scaling was performed using "ScaleData," with "S.Score," "G2M.Score" and "Stress" passed onto the "vars.to.regress" argument. At the same time, "nMUI" was also included in regression to control for the effects of cell size and/or sequencing depth.

Muscle.Score and Dev.Score
To readily detect skeletal muscle cells at various developmental or differentiation states, we assigned each cell a "Muscle.Score" using the above described "AddModuleScore" function using a list of conserved muscle cell genes (*PAX3*, *PAX7*, *PITX2*, *MYF5*, *MYF6*, *MYOD1*, *MYOG*, *NEB* and *MYH3*). To quantify the developmental status of myogenic progenitor and stem cells, we first used "AddModuleScore" to assign each cell a postnatal score ("Pst.Score") using genes that were found to be upregulated in stage 5 SCs compared to stage 1 and 2 embryonic SMPCs (Figure 4; Table S3). Similarly, we assigned each cell an embryonic score ("Emb.Score") using genes upregulated in stage 1 and 2 SMPCs compared to stage 5 SCs. Finally, we calculated each cell's myogenic developmental score ("Dev.Score") by subtracting its "Emb.Score" from "Pst.Score." Thus, a cell with a developmental "age" close to postnatal SCs would have a higher value of "Dev.Score," and that similar to embryonic SMPCs a lower value.

Dimensional reduction and clustering
First, the most highly variable genes within each Seurat object were calculated and selected using "FindVariableGenes" (1500-2500 genes). Principle components (PCs) were calculated using the selected top variable genes by "RunPCA," and the PCs were plotted using "PCElbowPlot." Significant PCs were selected based on the elbow plot and used to further reduce data dimensionality using the T-distributed stochastic neighbor embedding (tSNE) method by "RunTSNE." Cell clustering was performed by a shared nearest neighbor (SNN) modularity optimization based clustering algorithm using the Seurat function "FindClusters" with "reduction.type" set to "pca." Identification of clusters/cell types were aided by known cell type specific markers as well as the distribution of cells on the tSNE space.

Differential gene expression analysis
Differentially expressed genes (DEGs) between one cell cluster versus all remaining cells or between individual clusters were identified by "FindAllMarkers" or "FindMarkers," respectively. For both functions, "test.use" was set to "negbinom" to fit for the sparse data type generated from scRNA-seq, and "return.thresh" (*p* values) less than 0.01 (finding cluster markers) or 0.05 (comparing two clusters). We passed the same parameters as we did when scaling the data ("S.Score," "G2M.Score," "Stress" and "nUMI") to the "latent.var" argument to regress out the effects of cell cycle, dissociation-related stress as well as cell size/sequencing depth on the identification of DEGs. In addition, DEGs must also meet the following default criteria in Seurat: 1) average expression difference exceeding 1.28-fold between the comparing group of cells ("logfc.threshold = 0.25"), and 2) detected in a minimum of 10% of cells in either of the comparing populations ("min.pct = 0.1").

Trajectory analysis
For trajectory analysis, we reduced the dimensionality of the data by diffusion map (DM) (Haghverdi et al., 2015) using the top variable genes of the objects via the Seurat "RunDiffusion" function. For *in vivo* SMPC and SC only analysis, we further clustered the cells

using "FindClusters" with "reduction.type = "dm" (using the first 2 DM dimensions) into distinct developmental stages. For analysis combining *in vivo* SMPCs and SCs as well as hPSC-SMPCs, "RunDiffusion" was performed using the top variable genes from the *in vivo* only dataset as a reference gene set. The developmental stage labels of the *in vivo* cells and the sample identities of the hPSC-derived cells were transferred and maintained from the original objects.

Analysis using Monocle3

Analysis in the Monocle3 R package (Cao et al., 2019) was performed according to Trapnell lab guidelines (https://cole-trapnell-lab. github.io/monocle3/). Gene expression data and cell metadata including cell type labels were carried over from the Seurat object. Parameters to regress were set similarly to analysis in Seurat by passing "nUMI," "S.Score" "G2M.Score" and "Stress" to the "residual_model_formula_str" argument in the "preprocess_cds" function. Significant PCs were calculated and selected to further reduce the data dimensionality using uniform manifold approximation and projection (UMAP). Cells were plotted onto the UMAP space for visualization of their distribution and cell type identities.

Gene ontology enrichment analysis

Gene ontology (GO) enrichment was performed using Metascape (http://metascape.org/gp/index.html#/main/step1) (Zhou et al., 2019) against GO terms belonging to "Biological Processes." Enriched GO terms with similar properties were further assigned to a common group, and the top 20 groups were retrieved. Select representative GO terms (members) from the consolidated groups were plotted against their negative Log10-transformed *p* values (no more than one member was selected from each group).

Gene set enrichment analysis

The gene set enrichment analysis (GSEA) (https://www.gsea-msigdb.org/gsea/index.jsp) (Subramanian et al., 2005) was performed with the "GSEAPreranked" mode against the "Canonical Pathways" (c2.cp.v6.1) gene sets database. The "enrichment statistic" was set to "classic" and enriched gene sets containing more than 500 or less than 10 genes were excluded from the final enriched gene sets. The "normalization mode" was set to "meandiv" and permutations were performed 1000 times.

Co-regulated gene network analysis

To build the co-regulated gene network, the dataset containing all stages of *in vivo* SMPCs and SCs and *in vitro* hPSC-SMPCs derived using the HX protocol (Figure 7A), was used to compute a Pearson gene-to-gene correlation matrix and determine groups/networks including genes with correlation values greater than 0.125. Similar networks were condensed by segregation of cells into ample numbers of small cell clusters (roughly 50 cells per cluster), from which the expression of the primary networks was calculated and compared to each other again via a Pearson network-to-network correlation matrix, followed by merging similar networks with expression correlation of 0.7 or higher to generate the final networks. The expression level of a given gene group/network was calculated by averaging the normalized expression values of all genes in the group in a given cell. We manually inspected the gene groups to exclude those that were driven by an extremely high expression level of a few genes in random rare cells. To retrieve TFs from the gene groups, we intersected our identified genes with those annotated as transcription factors/regulators by the Animal Transcription Factor Database (bioinfo.life.hust.edu.cn/AnimalTFDB/). To mitigate the effects of tissue/cell dissociation-induced stress signatures, we compiled a common stress gene list (411 genes; Table S7) from published literature. Genes included in this list were chosen based on the following criteria: 1) included in the stress regression gene list as described above, or 2) significantly changed in the same direction (both induced or reduced) in response to dissociation-related stress as reported by van Velt-hoven et al. and Machado et al. (Machado et al., 2017; van Velthoven et al., 2017). Mouse genes were converted to their homologs in human and those mice only genes were removed from the final list. These common stress genes were intersected with the gene groups and TF sub-lists to exclude them from the final gene/TF lists for downstream analysis.

For gene group heatmaps, the average expression of selected groups was calculated for each developmental or directed differentiation stage/sample using the Seurat "AverageExpression" function. Only groups containing 50 or more genes were plotted. For GO analysis, all genes contained in a given group were used as input to Metascape for enrichment analysis against "GO Biological Processes."

Hierarchical clustering

Average gene expression levels of single cells belonging to the same groups were calculated using the Seurat "AverageExpression" function. Spearman correlation coefficients were calculated between the averaged group of cells and visualized using the R package pheatmap. Hierarchical clustering was performed via the same package with default settings.

Gene list intersection and Venn diagram generation

Individual gene lists were supplied as input to the R package eulerr. All possible intersections of input gene lists were calculated and visualized in Venn diagram format with region areas proportional to the number of events in the regions.

Update

Cell Stem Cell

Cell Stem Cell

Correction

A Human Skeletal Muscle Atlas Identifies the Trajectories of Stem and Progenitor Cells across Development and from Human Pluripotent Stem Cells

Haibin Xi, Justin Langerman, Shan Sabri, Peggie Chien, Courtney S. Young, Shahab Younesi, Michael Hicks,
Karen Gonzalez, Wakana Fujiwara, Julia Marzi, Simone Liebscher, Melissa Spencer, Ben Van Handel, Denis Evseenko,
Katja Schenke-Layland, Kathrin Plath,* and April D. Pyle*
*Correspondence: kplath@mednet.ucla.edu (K.P.), apyle@mednet.ucla.edu (A.D.P.)
https://doi.org/10.1016/j.stem.2020.06.006

(Cell Stem Cell 27, 158–176.e1–e10; July 2, 2020)

It came to our attention that during revision we updated the tSNE plot for the left panel of Figure 1D but mistakenly did not update the right panel of Figure 1D or Figure S1D. This error on our part does not affect any of the results or conclusions of our paper. The above-mentioned figures have now been updated with the correct tSNE coordinates and reproduced below. We apologize for this oversight and any inconvenience the readers might have encountered.
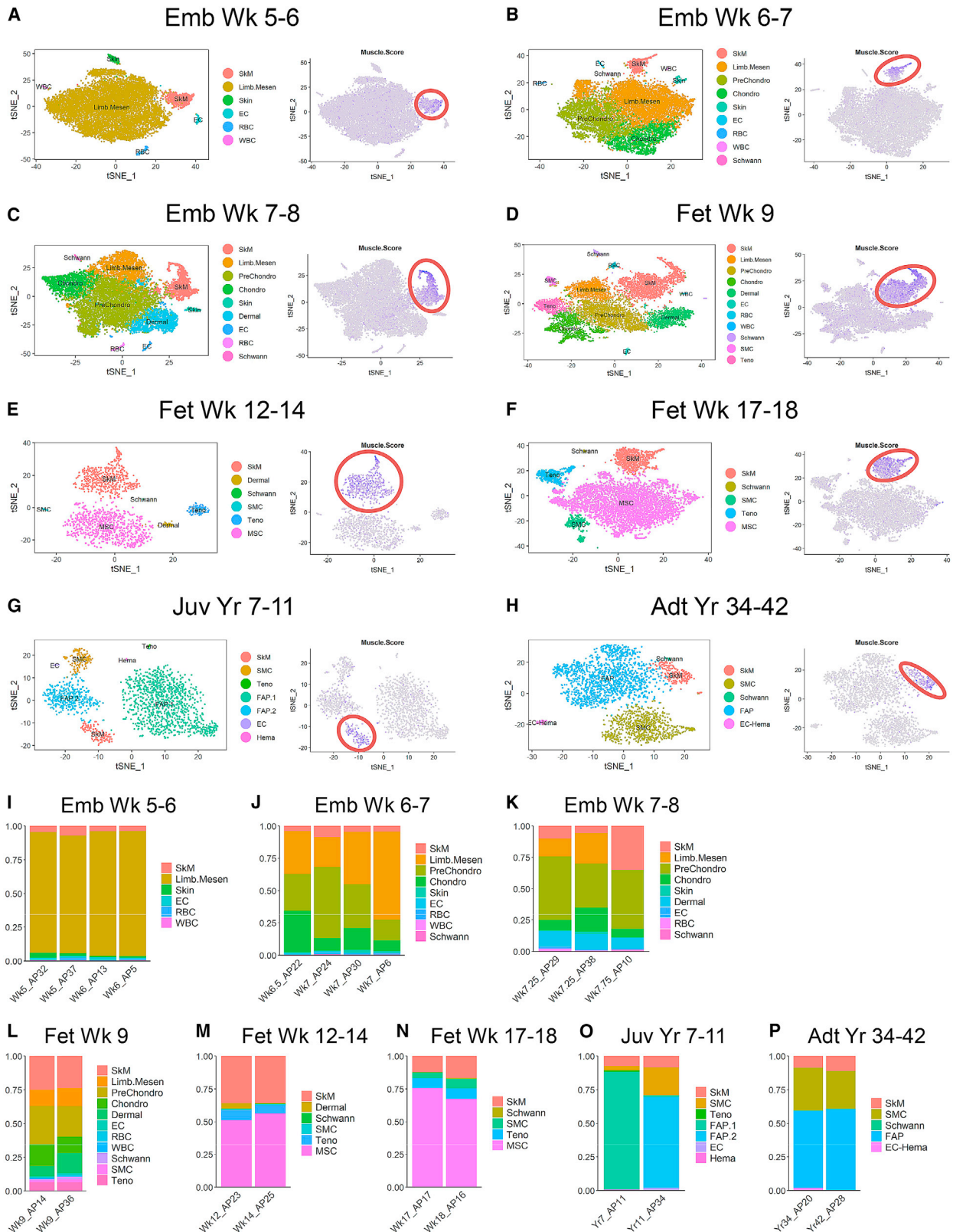
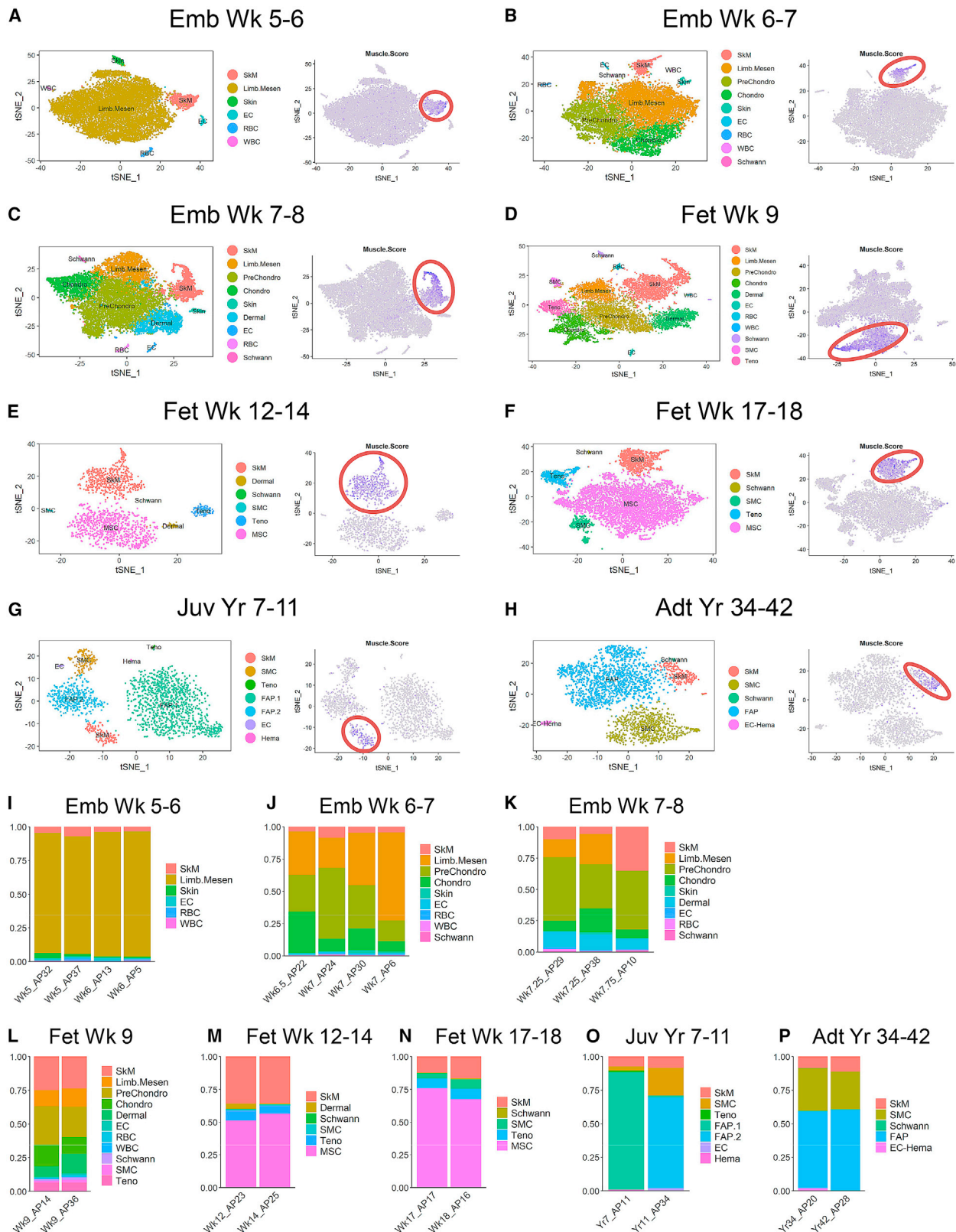Figure 1. ScRNA-Seq Identifies Dynamic Cell Types across Human Limb Development, corrected

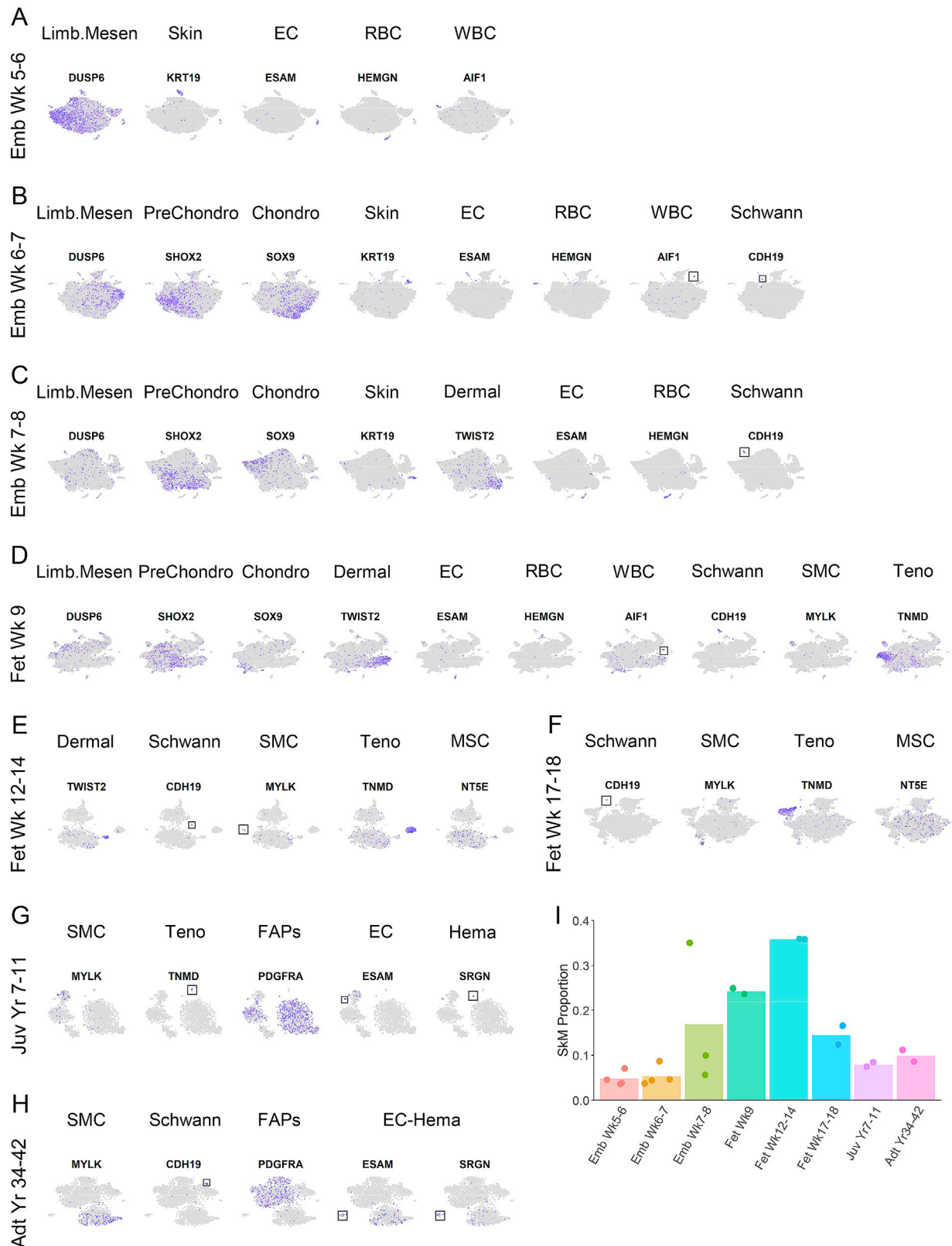Figure 1. ScRNA-Seq Identifies Dynamic Cell Types across Human Limb Development, original

Figure S1. Cell Types Present in Limbs and Skeletal Muscle Tissues at Different Human Developmental Stages, Related to Figure 1, corrected
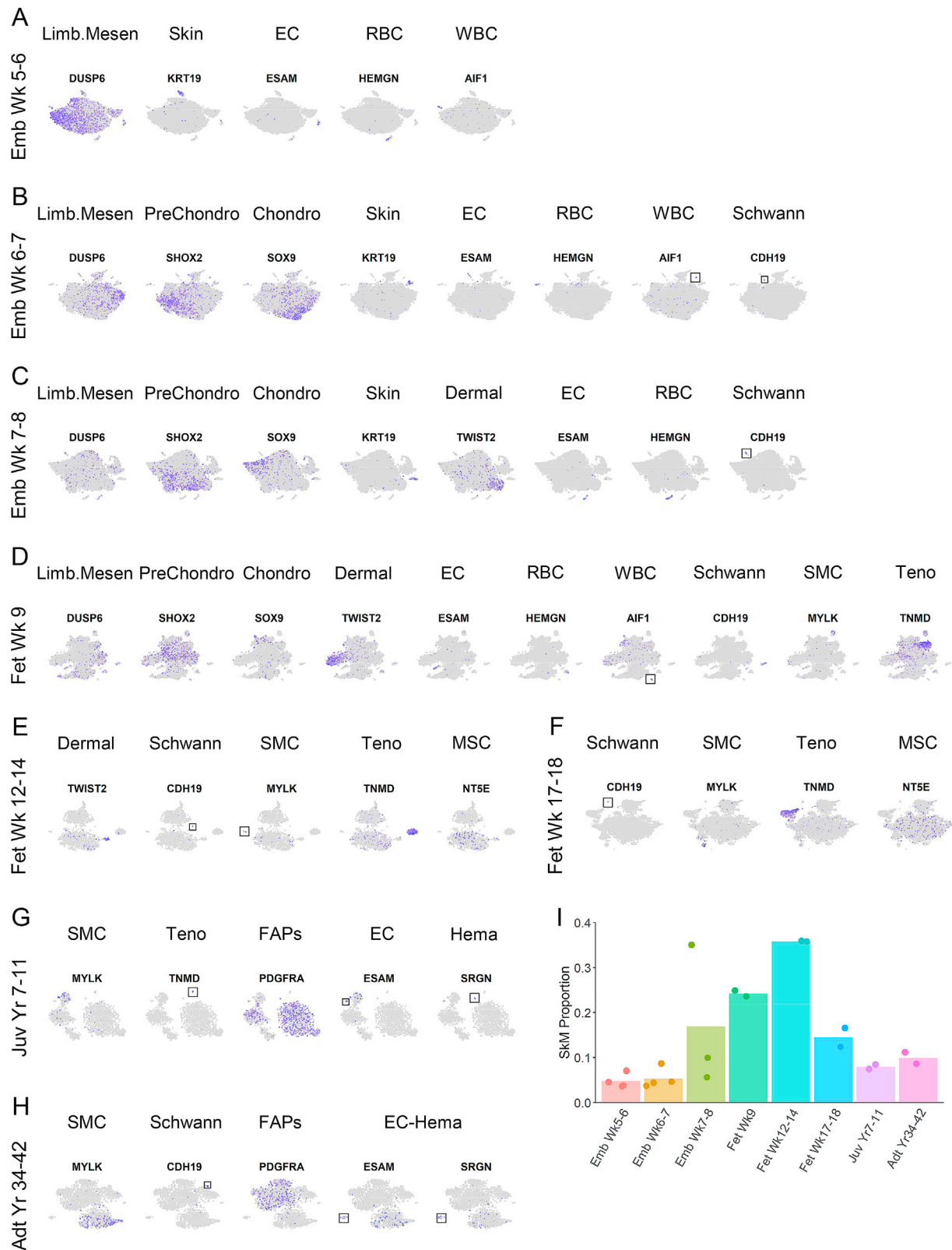
Figure S1. Cell Types Present in Limbs and Skeletal Muscle Tissues at Different Human Developmental Stages, Related to Figure 1, original